

1 **Investigating beach erosion related with tsunami sediment transport at Phra Thong Island,**  
2 **Thailand caused by the 2004 Indian Ocean tsunami**

3  
4 Ryota Masaya<sup>1</sup>, Anawat Suppasri<sup>2</sup>, Kei Yamashita<sup>2</sup>, Fumihiko Imamura<sup>2</sup>, Chris Gouramanis<sup>3</sup>  
5 and Natt Leelawat<sup>4,5</sup>

6 <sup>1</sup>Civil and Environmental Engineering, Graduate School of Engineering, Tohoku University, 6-6-06  
7 Aoba, Aramaki-Aza, Aoba, Sendai 980-0845, Japan

8 <sup>2</sup>International Research Institute of Disaster Science, Tohoku University, 468-1 Aoba, Aramaki-Aza,  
9 Aoba, Sendai 980-0845, Japan

10 <sup>3</sup>Department of Geography, National University of Singapore, 1 Arts Link, Singapore 117570, Singa-  
11 pore

12 <sup>4</sup>Department of Industrial Engineering, Faculty of Engineering, Chulalongkorn University, Phayathai  
13 Road, Pathumwan, Bangkok 10330, Thailand

14 <sup>5</sup>Disaster and Risk Management Information Systems Research Group, Chulalongkorn University, Pha-  
15 yathai Road, Pathumwan, Bangkok 10330, Thailand

16 \*Corresponding author.

17 *E-mail address:* ryota.masaya.r6@dc.tohoku.ac.jp (Ryota Masaya)

18  
19 **Abstract**

20 The 2004 Indian Ocean Tsunami and the 2011 Great East Japan earthquake and tsunami caused large-  
21 scale topographic changes in coastal areas. Whereas much research has focused on coastlines that have  
22 or had large human populations, little focus has been paid on coastlines that have little or no infrastruc-  
23 ture. The importance of examining erosional and depositional mechanisms of tsunami events lies in the  
24 rapid **reorganization** that coastlines must undertake immediately after an event. A thorough understand-  
25 ing of the pre-event conditions is paramount to understanding the natural reconstruction of the coastal  
26 environment. This study examines the location of sediment erosion and deposition during the 2004  
27 Indian Ocean Tsunami event on the relatively pristine Phra Thong Island, Thailand. Coupled with sat-  
28 ellite imagery, we use numerical simulations and sediment transportation models to determine the loca-  
29 tions of significant erosion and the areas where much of that sediment was redeposited during the tsu-  
30 nami inundation and backwash processes. Our modelling approach suggests that beaches located in two  
31 regions on Phra Thong Island were significantly eroded by the 2004 tsunami, predominantly during the  
32 backwash phase of the first and largest wave to strike the island. Although 2004 tsunami deposits are  
33 found on the island, we demonstrate that most of the sediment was deposited in the shallow coastal area,  
34 facilitating quick recovery of the beach when normal coastal processes resumed.

35  
36 **1. Introduction**

37 The 2004 Indian Ocean Tsunami and the 2011 Great East Japan earthquake and tsunami caused large-  
38 scale geomorphologic changes in coastal areas during the erosional phases of inflow and outflow (Pari

39 et al., 2008; Goto et al., 2011a; Tanaka et al., 2011; Haraguchi et al., 2012; Hirao et al., 2012; Udo et  
40 al., 2013; Imai et al., 2015). In each tsunami event, the erosional phases translocated sediments onshore  
41 and offshore, and primed the coastal zone for rapid (months to decades) recovery (Choowong et al.,  
42 2009; Ali and Narayama, 2015; Udo et al., 2016; Mieda et al., 2017; Koiwa et al., 2018). However, little  
43 information exists to identify real-time sediment dynamics during the erosional and depositional phases  
44 of tsunami events. In particular, erosive phases mobilize sediments into the onshore (e.g. Jankaew et al.  
45 2008; Gouramanis et al. 2017) and offshore environments (e.g. Feldens et al 2009). Following the tsu-  
46 nami event, both offshore environment and coastal environments are primed for natural processes to  
47 resume and redistribute sediments onshore to restore the coastal environment to similar pre-tsunami  
48 configurations.

49 However, in many regions, such as the area affected by the 2011 tsunami, extensive engineering  
50 interventions (e.g. levee construction and land level raising) are affecting the natural recovery processes  
51 of the coastal zone. In Japan, plans for coastal reconstruction and defenses are typically formulated  
52 shortly after a tsunami, preventing natural recovery processes (Suppasri et al., 2016) and many locations  
53 have not undergone or been allowed to recover naturally (Udo et al., 2016). These political and engi-  
54 neering interventions make it difficult to observe or predict the natural recovery processes of coastal  
55 areas.

56 Before an understanding of the recovery processes of a tsunami-affected coastal zone can be  
57 achieved, a thorough understanding of the sediment budget must be determined. The relocation of sed-  
58 iments during the main tsunami erosion and deposition phases establishes the pre-recovery or baseline  
59 conditions upon which natural processes can act to facilitate the recovery of the coastal zone. To deter-  
60 mine the locations of sediment deposition during a tsunami event, the sediment transport dynamics  
61 during the tsunami must be defined.

62 Unfortunately, real-time data from observations has not been possible to establish quantitative esti-  
63 mates of sediment erosion and deposition during a tsunami event, though qualitative spatial patterns of  
64 sediment process (Udo et al., 2016; Yamashita et al., 2016) have been examined through analyze of  
65 video footage. Prior studies have mainly estimated sediment transport dynamics, such as erosion and  
66 sediment deposition through remote sensing (e.g. Fagherazzi and Du 2008, Choowong et al., 2009;  
67 Liew et al., 2010), and sedimentological and stratigraphic analysis (e.g. Paris et al. 2007; Hawkes et al.  
68 2007; Switzer et al. 2012). However, the information obtained regarding the final results of the sediment  
69 transport process is limited. It is difficult to obtain information on where sediment has eroded and de-  
70 posited (e.g. Pham et al., 2018), and whether topographic changes caused by the local sediment runoff  
71 or deposition are the results of action from inflow or backwash (e.g. Choowong et al., 2009; Paris et al  
72 2007; Switzer et al. 2012). This information determines the sediment budget in the system before and  
73 after the tsunami and is therefore important for considering geomorphic recovery.

74 Numerical simulations using wave dynamics of an area can reproduce spatial-temporal variations of  
75 the sediment mobility and deposition and can effectively model the sediment transport process using  
76 the wave and sediment characteristics of the natural system. In recent years, the numerical modeling of

77 tsunami sediment transport has been developed (e.g. Takahashi et al., 2000), improved (e.g. Takahashi  
78 et al., 2011; Apotsos et al., 2011a; Li et al., 2013; Morishita and Takahashi, 2014; Yamashita et al.,  
79 2018) and applied in the field (e.g. Gelfenbaun et al., 2007; Takahashi et al., 2008; Apotsos et al., 2011b;  
80 Apotsos et al., 2011c; Gusman et al., 2012; Li et al., 2014; Arimitsu et al., 2017; Yamashita et al., 2017),  
81 and reproducibility has been confirmed by comparison between the calculated and measured values  
82 (e.g. Li et al., 2012; Ranasinghe et al., 2013; Sugawara et al., 2014a; Yamashita et al., 2015; Yamashita  
83 et al., 2016).

84 An important consideration in the sediment dynamics during catastrophic marine events (e.g. typhoon  
85 and tsunami) is the degree of development and human modification of the coastal zone prior to the  
86 event. Artificial structures, such as sea walls, roads and buildings interfere with washover processes,  
87 and these areas are often targeted from reconstruction and rehabilitation through rapid engineering re-  
88 construction. Little is known about the recovery processes in sparsely developed and unpopulated areas.  
89 As such, the largely, anthropogenically-undisturbed Phra Thong Island, western Thailand, is an ideal  
90 location to model the sediment dynamics, coastal erosion and deposition following a major tsunami  
91 event.

92 The main objective of this study is to investigate the **short-term** conditions of sediment transport such  
93 as erosional and depositional process and establishes the baseline sediment conditions that led to further  
94 investigation of the **long-term** recovery of the Phra Thong Island coastline after the 2004 IOT. We used  
95 tsunami sediment transport calculations to spatio-temporally reproduce the sediment transport pro-  
96 cesses occurring during the tsunami and identify zones of sediment deposition in the offshore and on-  
97 shore areas and validate these modelling results with published observational data of the 2004 IOT  
98 deposits on the island. Due to the largely natural environment, Phra Thong Island is a rare case that is  
99 useful for verifying tsunami sediment transport models where few artificial features can generate model  
100 uncertainties.

101 Examining the sediment transport processes on Phra Thong Island is also expected to elucidate phe-  
102 nomena, improve numerical calculation models for the future and is applicable to other areas. Further-  
103 more, at least three palaeotsunami deposits were identified in areas impacted by the 2004 IOT on Phra  
104 Thong Island (Jankaew et al., 2008; Sawai et al., 2009; Fujino et al., 2009; Fujino et al., 2010; Prender-  
105 gast et al. 2012; Brill et al., 2012a, b; Gouramanis et al., 2017; Pham et al., 2018). Thus, clarifying the  
106 sediment transport conditions of the 2004 tsunami will also be important for future estimations of his-  
107 tory, scope and cause of older tsunamis on Phra Thong Island and elsewhere in the coastal areas of the  
108 Indian Ocean.

109

## 110 **2. Setting and method**

### 111 **2.1. Phra Thong Island, Thailand**

112 During the 2004 IOT, a wave of approximately 7 m inundated the northern portion of Phra Thong Island  
113 (Fig. 1) and measurements up to 20 m were recorded from the southernmost tip of the island (Jankaew  
114 et al. 2008). Over 70 people were lost and a village of 100 households disappeared. Geomorphologically,

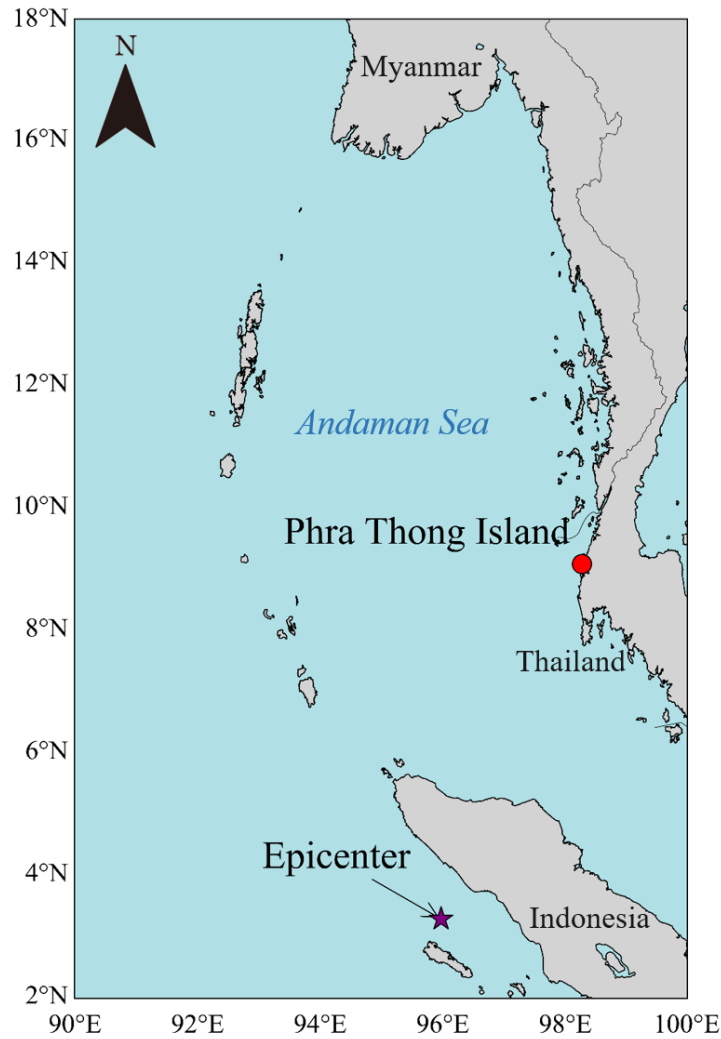


Figure 1 Location of Phra Thong Island

115

116

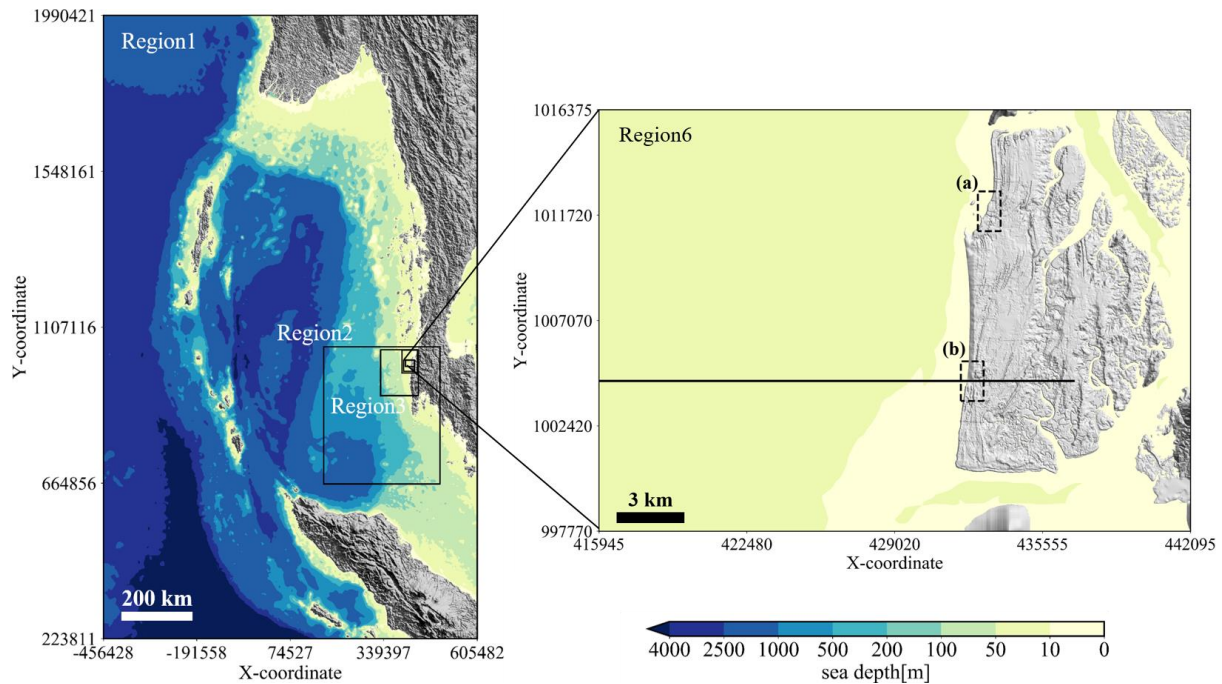
117

118 the western coast of the island has a beach ridge sequence trending parallel to the coast, which formed  
 119 during the sea level regression following mid-Holocene sea level highstand **about 6,000 B.P.** (Brill et  
 120 al. 2015). The eastern shore of the island is extensively covered by mangroves along the shores of tidal  
 121 channels. The island has a tropical climate. Additionally, palaeotsunami deposits are preserved in swales  
 122 in the beach ridge system along the western coast of Thailand (e.g. Jankaew et al. 2008; Gouramanis et  
 123 al. 2017). Furthermore, although local beaches were lost in the 2004 tsunami, satellite photography  
 124 showed rapid natural recovery within 18 months (e.g. Choowong et al. 2009).

125

## 126 **2.2. Topography and bathymetry data**

127 The topography and bathymetry data used for the tsunami sediment transport calculations were cre-  
 128 ated based on various water depths and elevations. Figure 2 shows the terrain data that were created.  
 129 Topographic data were downscaled from Region 1, which includes the Andaman Sea, to Region 6,  
 130 which includes all of Phra Thong Island. The grid spacing decreases from Region 1 (the spatial grid  
 131 size  $\Delta x_1 = 1,215$  m) to Region 6 ( $\Delta x_6 = 5$  m). In the tsunami sediment transport calculations, UTM zone



132

133 Figure 2 Terrain data (The black frame shows Region 1 to Region 6, and the black line in Region 6  
 134 shows the cross-section where calculation was performed. Dashed squares are the beach where ero-  
 135 sion was confirmed from satellite image.)

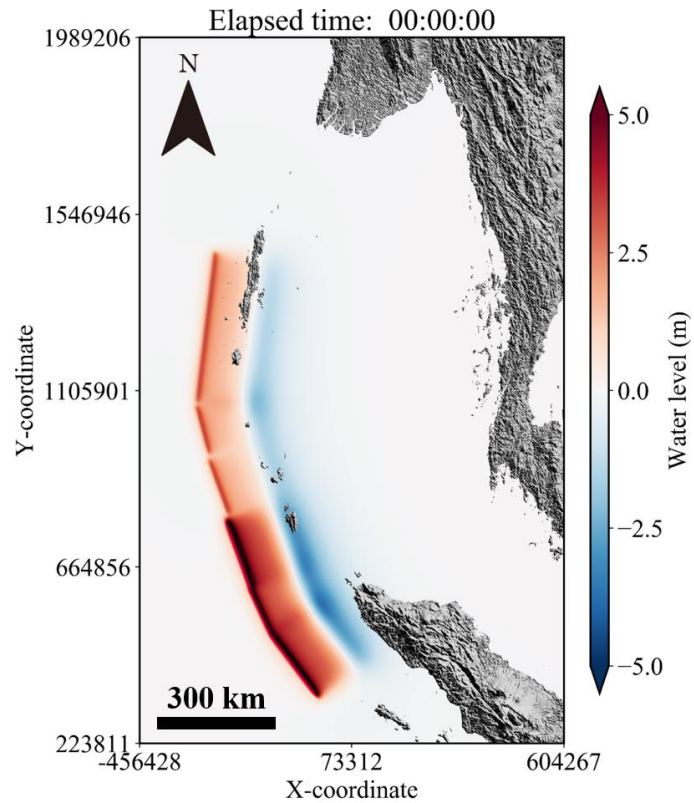
136

137 47N was used to geospatially constrain the horizontal modelling coordinates of Phra Thong Island.  
 138 Region 1 is the projection of depth data of the 30-second grid provided by GEBCO (2014) on the Car-  
 139 tesian coordinate system UTM 47N. Regions 2–4 use a digital marine chart with 300 m resolution based  
 140 on a survey by the Royal Thai Navy. Regions 5 and 6 use an original 5 m (terrain data) and 15 m (sea  
 141 depth data) grid spacing to create mean terrain and water depth data based on analysis of satellite image  
 142 by EOMAP and elevation data provided by the Land Development Department of Thailand (LDD,  
 143 2018). The terrain data of Region 4, created from the digital marine chart of 300 m resolution, showed  
 144 discontinuity at the boundary with Region 5, which had a higher resolution. The discontinuity was  
 145 therefore removed to the extent possible by interpolation with an inverse distance weighting method  
 146 using all terrain data.

147

### 148 **2.3. Tsunami source model**

149 The tsunami source model proposed by Suppasri et al. (2011) was used as the tsunami source of the  
 150 2004 Indian Ocean Tsunami as the model focused on the coast of Thailand and accurately reproduced  
 151 the inundation area and surveyed trace height of the 2004 IOT. The fault model is divided into six small  
 152 faults from satellite image analysis and survey results, and it is assumed that each small fault slides  
 153 simultaneously and instantaneously. For the tsunami source, the vertical tectonic displacement in each  
 154 fault was calculated according to Okada (1985). Table 1 shows the fault parameters of each fault and  
 155 Figure 3 shows the initial water level.



156

157

Figure 3 Initial water level after earthquake occurrence

158

159

Table 1 Earthquake fault parameters for calculating initial water level (Suppasri et al., 2011)

Segment No.	1	2	3	4	5	6
Latitude (°N)	3.03	4.48	5.51	7.14	8.47	9.63
Longitude (°E)	94.4	93.3	92.9	92.3	91.9	91.6
Strike (deg)	323	335	340	340	345	7.00
Dip (deg)	15.0	15.0	15.0	15.0	15.0	15.0
<b>Rake</b> (deg)	90.0	90.0	90.0	90.0	90.0	90.0
Length (km)	200	125	180	145	125	380
Width (km)	150	150	150	150	150	150
<b>Slip</b> (m)	14.0	12.6	15.1	7.00	7.00	7.00
Depth (km)	10.0	10.0	10.0	10.0	10.0	10.0

160

## 161 **2.4. Tsunami sediment transport calculation**

### 162 **2.4.1. Tsunami propagation and run-up model**

163 Tohoku University's Numerical Analysis Model for Investigation of Near-field tsunamis, No. 2

164 (TUNAMI-N2) is based on the nonlinear long wave theory and was used as the tsunami propagation

165 and run-up model (Imamura, 1996).



166 
$$\frac{\partial \eta}{\partial t} + \frac{\partial M}{\partial x} + \frac{\partial N}{\partial y} = 0 \quad (1)$$

167

168 
$$\frac{\partial M}{\partial t} + \frac{\partial}{\partial x} \left( \frac{M^2}{D} \right) + \frac{\partial}{\partial y} \left( \frac{MN}{D} \right) + gD \frac{\delta \eta}{\delta x} + \frac{gn^2}{D^{\frac{7}{3}}} M \sqrt{M^2 + N^2} = 0 \quad (2)$$

169

170 
$$\frac{\partial N}{\partial t} + \frac{\partial}{\partial x} \left( \frac{MN}{D} \right) + \frac{\partial}{\partial y} \left( \frac{N^2}{D} \right) + gD \frac{\delta \eta}{\delta y} + \frac{gn^2}{D^{\frac{7}{3}}} N \sqrt{M^2 + N^2} = 0 \quad (3)$$

171

172 Here,  $\eta$  is the change in water level from the still-water surface,  $D$  is the total water depth from the  
 173 bottom to the water surface, and  $g$  is the acceleration of gravity. The bottom friction is expressed ac-  
 174 cording to the Manning formula, where  $n$  is Manning's roughness coefficient ( $n = 0.025 \text{ s m}^{-1/3}$ ).  $M$  and  
 175  $N$  are the total flow fluxes in the  $x$  and  $y$  directions, respectively, and are given by integrating the hori-  
 176 zontal flow velocity  $u, v$  from the water bottom  $h$  to the water surface  $\eta$ . It is assumed that the horizontal  
 177 flow velocity is uniformly distributed in the vertical direction.

178 The nonlinear long wave theory consists of a continuous equation that is derived from (1) the princi-  
 179 ple of conservation of mass (continuity equation) and (2) the conservation of momentum (equation of  
 180 motion). These two equations are obtained by vertically integration from the seabed to the water surface.

181 When the water depth is about 50 m or less, the effects of the **second, third and fifth** terms of the  
 182 advection and seabed friction terms (Equations 2 and 3) are reduced, therefore wave theory that omit  
 183 these terms is often used at depths shallower than 50 m. Meanwhile, the Message Passing Interface  
 184 (MPI) parallel was implemented in the model for highly efficient calculations. Both the advection term  
 185 and the bottom friction term were therefore considered in the calculations without reducing accuracy in  
 186 deeper waters.

187 The reproducibility of the calculated results is based on the tsunami height data (IUGG; available at  
 188 <http://www.nda.ac.jp/~fujima/TMD/index.html>) for the 2004 IOT and is discussed using the geometric  
 189 mean  $K$  and geometric standard deviation  $\kappa$  proposed by Aida (1978).

190

191 
$$\log K = \frac{1}{n_p} \sum_{i=1}^n \log K_i \quad (4)$$

192

193 
$$\log \kappa = \sqrt{\frac{1}{n_p} \left\{ \sum_{i=1}^n (\log K_i)^2 - n_p (\log K)^2 \right\}} \quad (5)$$

194

195 Here,  $n_p$  is the number of points,  $R_i$  is the tsunami height at the  $i$ th point,  $H_i$  is the calculated value at

196 the  $i$ th point, and  $K_i = R_i/H_i$ .

197

#### 198 **2.4.2. Sediment transport model**

199 For the tsunami movable bed model, we used the numerical Sediment Transport Model (STM) pro-  
200 posed by Takahashi et al. (2000), which solves the time evolution of sediment transport considering the  
201 exchange sediment volume of the bed and suspended load layers according to the flow conditions of  
202 the nonlinear long wave theory-based TUNAMI-N2 model. For each time step in the finest calculation  
203 region (region 6), the STM receives the total flow fluxes from TUNAMI-N2 and calculates the change  
204 of seafloor and land surface and feeds this to the next time step of the TUNAMI-N2 model.

205 **In this model, tsunami sediment transportation is derived into two layers, bed load layer and sus-**  
206 **suspended load layer. In the bed layer, the sediment particles are transported through rolling, sliding or**  
207 **saltating. In the suspended load layer, the sediment particles are uplifted and transported by the dynamic**  
208 **of flowing suspension.** The governing equations consist of continuous equations for the bed load layer  
209 and the suspended load layer:

210

$$211 \quad \frac{\partial Z_B}{\partial t} + \frac{1}{1 - \lambda} \left( \frac{\partial q_{B,x}}{\partial x} + \frac{\partial q_{B,y}}{\partial y} + w_{\text{ex}} \right) = 0 \quad (6)$$

212

$$213 \quad \frac{\partial Ch_s}{\partial t} + \frac{\partial CM}{\partial x} + \frac{\partial CN}{\partial y} - w_{\text{ex}} = 0 \quad (7)$$

214

215 Here,  $\lambda$  is the **porosity of the sand particles**,  $Z_B$  is the bottom height from the reference plane,  $q_B$  is the  
216 amount of bed load sediment,  $C$  is the average suspended load layer concentration,  $h_s$  is the suspended  
217 load layer thickness (= total water depth), and  $M$ ,  $N$  are the water discharges in the  $x$  direction and  $y$   
218 direction,  $w_0$  is the **settling velocity of the sand particles**.

219 Equation (6) is a continuous equation for within the bed load layer. The first term is the exchange  
220 sediment volume with the bottom, the second term is the balance of sediment flow volume moving in  
221 a tractive form in the flow direction, and the third term defines the balance of suspension flux, caused  
222 by diffusion, and sedimentation flux, caused by gravity, as the exchange sediment volume between the  
223 bed load layer and the suspended load layer.

224 Equation (7) is a continuous equation for within the suspended load layer. The first and second terms  
225 are bed load sediment moving in a suspended state in the flow direction, the third term is the exchange  
226 sediment volume between the bed load layer and the suspended load layer, and the fourth term is the  
227 increase or decrease of the sediment flow in the suspended load layer.

228 In Equations (8) and (9), the equations defining the bed load sediment volume  $q_B$  and the equation  
229 defining the exchange sediment volume  $w_{\text{ex}}$  of the bed load layer and suspended load layer are neces-  
230 sary, but according to Takahashi et al. (2000), they are obtained by the following:

231



232 
$$q_{B,x y} = \alpha \sqrt{sgd^3} (\tau^* - \tau_{crit}^*)^2 \quad (8)$$

233  
234 
$$w_{ex} = \beta \sqrt{sgd} (\tau^* - \tau_{crit}^*)^2 - w_0 C \quad (9)$$

235  
236 
$$\tau_* = \frac{u^{*2}}{sgd} \quad (10)$$

237  
238 Here,  $\alpha$  is the coefficient of the bed load sediment volume equation,  $\beta$  is the coefficient of the suspension  
239 volume equation,  $s$  is the submerged density of the sand particles ( $s = \rho_s / \rho_w - 1$ ;  $\rho_s$  and  $\rho_w$  are the  
240 density of sand particles and water, respectively;  $\rho_s = 2,650 \text{ kg m}^{-3}$  and  $\rho_w = 1,000 \text{ kg m}^{-3}$ ,  $g$  is  
241 the acceleration of gravity,  $d$  is the grain diameter,  $w_0$  is the settling velocity of the sediment grains,  $\tau^*$   
242 is the Shields parameter (Equation (10)),  $\tau_{crit}^*$  is the critical Shields parameter,  $u^*$  is the friction ve-  
243 locity obtained from the Manning's law ( $u^{*2} = gn_s^2 M |M| / D^{7/3}$ ).  $n_s$  is the roughness coefficient for  
244 STM. It is worthwhile to mention that in the tsunami calculation, roughness coefficient  $n$  is the param-  
245 eter to calculate the shear stress from ground surface which is differs from  $n_s$ , the parameter for calcu-  
246 lating the shear stress which forces on the surface of sand particles.

247 The grain-size dependent parameter for bed load ( $\alpha$ ) and exchange rate ( $\beta$ ) in Equation (8) and (9)  
248 are derived from Equations (11) and (12) based on the hydraulic experiments by Takahashi et al. (2011):

249  
250 
$$\alpha = 9.8044e^{-3.366d} \quad (11)$$

251  
252 
$$\beta = 0.0002e^{-6.5362d} \quad (12)$$

253  
254 However, the functions should not be applied when  $d$  is outside the 0.166 mm to 0.394 mm range as he  
255 validity of extrapolated  $d$  values may produce erroneous results.

256  
257 
$$w_0 = \sqrt{sgd} \left( \sqrt{\frac{2}{3} + \frac{36v^2}{sgd^3}} - \sqrt{\frac{36v^2}{sgd^3}} \right) \quad (13)$$

258  
259 Equation (13) is a settling velocity of the sand particles by Rubey (1933). Here,  $\nu$  is the kinematic  
260 viscosity coefficient ( $\nu = 1.39 \times 10^{-6} \text{ m}^2 \text{ s}^{-1}$ ).

261 Considering the effect from the bed slope (Watanabe et al., 1984), the formulation of the bed load,  
262  $q_B$ , Equation (6), is rewritten as  $Q_B$  as shown in Equations (14) and (15):

263  
264 
$$Q_{B,x} = q_{B,x} - |q_{B,x}| \varepsilon \frac{\partial Z_B}{\partial x} \quad (14)$$

265

266

$$Q_{B,y} = q_{B,y} - |q_{B,y}| \varepsilon \frac{\partial Z_B}{\partial y} \quad (15)$$

267

268 where  $\varepsilon$  is the parameter which related to the diffusion coefficient of the sediments ( $\varepsilon = 2.5$ ; Sugawara  
269 et al., 2014a).

270

271

272

273

274

275

276

277

$$C_s = \frac{\rho_w}{\rho_s - \rho_w} \frac{e_s n_s^2 u^3}{h_s^{4/3} w_0 - e_s n_s^2 u^3} \quad (16)$$

278

279

280

281

282

283

284

285

where  $e_s$  is the efficiency coefficient ( $e_s = 0.025$ ; Bagnold, 1966). Note that in the sediment transport calculation, the saturation concentration of suspend sediments given by Equation (16) is applied entrainment of sediment from the bottom layer. Namely, sediment supply from the bottom to the water column (suspended load layer) by  $w_{ex}$  is not permitted if  $C \geq C_s$ . However, supersaturation ( $C \geq C_s$ ) due to sediment advection, or sudden decrease of  $C_s$  due to the change of flow parameters, is permitted. In this calculation, when  $C$  exceeds maximum concentration  $C_{max}$  was set to 37.7%, based on the observed value (Xu, 1999a, 1999b).

286

287

288

289

290

291

292

## 2.5. Calculation conditions

293

294

295

296

The initial conditions for the numerical simulations used the terrain data (Figure 2) and tsunami source (Figure 3). The simulations were performed using a 3:1 nested grid that increased the resolution a 1,215 m<sup>2</sup> grid to a 5 m<sup>2</sup> grid. Additionally, the target region of the sediment transport calculation was limited to Region 6, with a grid spacing of 5 m<sup>2</sup>.

297

298

299

300

The simulations were calculated over a 0.05 second increment with a 6-hour period in which the test case with a 12-hour period showed the suspended sediment concentration in the vicinity of the shoreline decreased and stabilized. Therefore, 6-hour simulation was used for the reproduction of the 2004 tsunami as well as further sensitivity analysis of the grain size and roughness coefficient.

301

Table 2 Set parameters for sediment transport calculations

Parameter	Value
Coefficient of bed load sediment volume equation $\alpha$	6.40
Coefficient of suspension sediment volume equation $\beta$	$8.70 \times 10^{-5}$
Critical friction velocity $u_{crit}^*$	0.0137 m s <sup>-1</sup>
Settling velocity of sand particles $w_0$	0.00971 m s <sup>-1</sup>

302

303 For the bottom conditions of STM, the roughness coefficient was fixed at  $n_s = 0.030 \text{ s m}^{-1/3}$ , and the  
304 entire area of Region 6 was considered the movable bed. In general, when simulating tsunami sediment  
305 transport, it is necessary to determine the roughness coefficient according to land use. However, since  
306 there is no land use map before the tsunami on Phra Thong Island, a fixed value was used, similar to  
307 previous studies (e.g. Sugawara et al., 2014a, b; Yamashita et al., 2015; Yamashita et al., 2016). How-  
308 ever, Sugawara et al. (2014a) showed that the variation in Manning's roughness coefficient for the sand  
309 beds may affect the general distribution pattern of sediment deposits and erosions across the artificial  
310 topographic features with much higher roughness coefficient such as artificial canals, roads and popu-  
311 lated residential areas. Therefore, a sensitivity analysis on the roughness coefficient was performed.  
312 Phra Thong Island has no such artificial topographic features and using the single roughness coefficient  
313 should sufficiently capture the overall roughness. However, to ensure robust conclusions, a sensitivity  
314 analysis for two bottom conditions was performed at  $n_s = 0.025 \text{ s m}^{-1/3}$  and  $n_s = 0.035 \text{ s m}^{-1/3}$ , which are  
315 within the range of previously used estimates of roughness (e.g. Sugawara et al., 2014a, b).

316 The grain size was based on one sediment data set (Gouramanis et al., 2017) from the locally eroded  
317 region, and was considered as a representative value for all of the tsunami sediment grain sizes. A uni-  
318 form grain size of  $d = 0.127 \text{ mm}$  was used. The critical Shields parameter  $\tau_{crit}^*$  in Equations (9) and  
319 (10) was obtained using Equations (17) and (18) according to Iwagaki et al. (1956):

320

$$321 \tau_{crit}^* = u_{crit}^{*2} \rho \quad (17)$$

322

$$323 u_{crit}^{*2} = 8.41 d^{\frac{11}{32}} \quad (18)$$

324

325 Here,  $u_{crit}^*$  is the critical friction velocity and  $\rho$  is the density of water. Table 2 shows each parameter  
326 used for the sediment transport calculations in this study.

327 The numerical model used in this paper can only consider a single grain size, so the model cannot  
328 resolve the grading observed in the sand layers (e.g. Gouramanis et al., 2017). Additionally, initial bed  
329 grain size can have a large effect on erosion and deposition (e.g. Apotsos et al., 2011b; Sugawara et al.,  
330 2014a; Jaffe et al., 2016). Furthermore, the sediment data we used to set the grain size is from a single  
331 location in the north of the island, and is assumed to be a representative grain size for the tsunami  
332 deposits. As such we performed a sensitivity analysis on the grain size. Pham et al. (2018) investigated

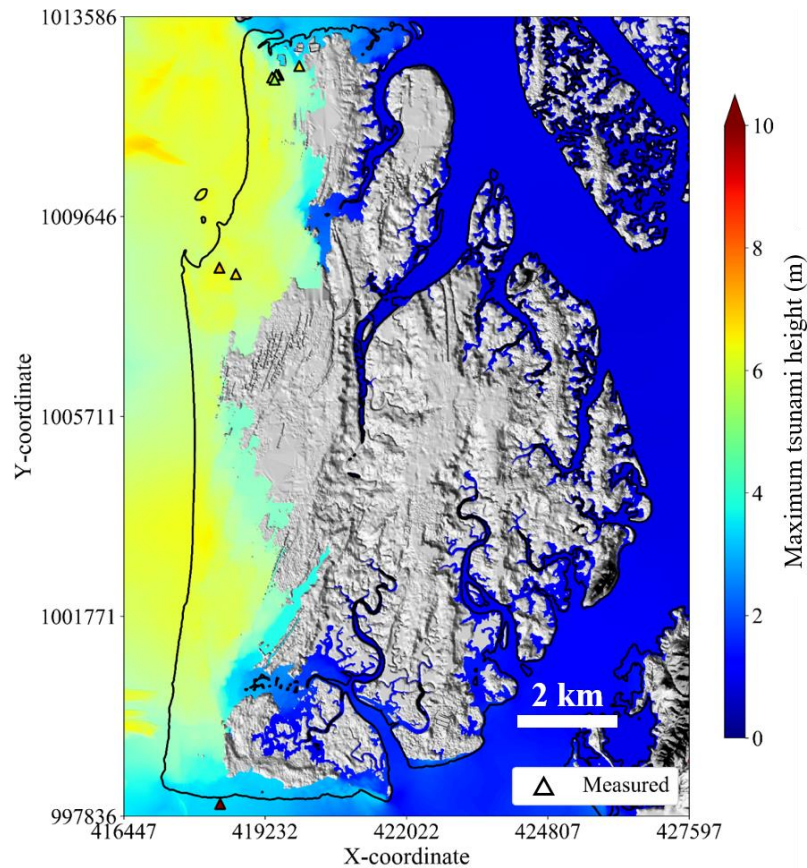


Figure 4 Comparison of calculated and measured maximum tsunami height

333  
334  
335

336 the surface grain size of the offshore (water depth > 15 m), nearshore (water depth < 15 m), and onshore  
337 on Phra Thong Island, which they considered to be the source of sediments that formed the tsunami  
338 deposits. Pham et al. (2018) recorded a mean grain size of 0.314 mm in the offshore area, 0.129 mm in  
339 the nearshore area, and 0.285 mm in the onshore area. Based on these mean grain sizes, we conducted  
340 a sensitivity analysis for two grain sizes (0.285 mm and 0.314 mm representing the offshore and onshore  
341 sediments).

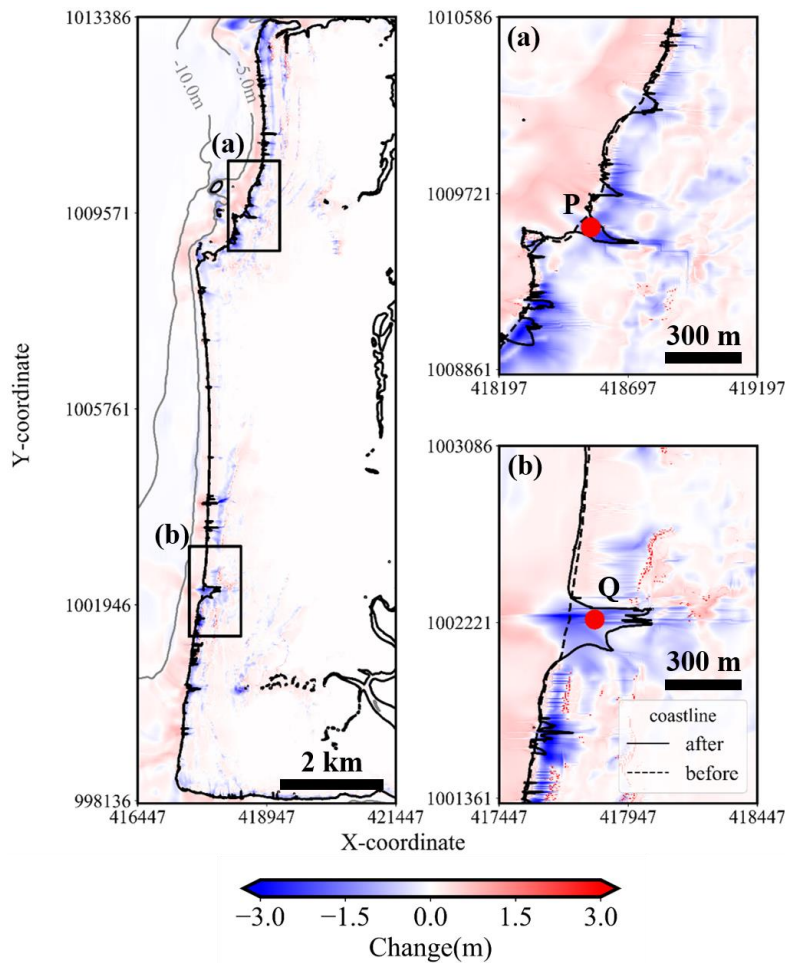
342

### 343 3. Results

#### 344 3.1. Verification of reproducibility

##### 345 3.1.1. Tsunami height

346 Figure 4 shows the results of the calculation of the maximum tsunami heights and the seven measured  
347 tsunami heights on Phra Thong Island. From Equations (4) and (5),  $K = 1.16$  and  $\kappa = 1.40$  are obtained.  
348 The Japan Society of Civil Engineers (2012) consider  $0.95 < K < 1.05$  and  $\kappa < 1.45$  as guides for eval-  
349 uating reproducibility of tsunami numerical calculations. Although the  $K$  value is slightly higher than  
350 the guideline but this is because of an uncertain 19.6 m measured in the southern part of the Island.  
351 Additionally, the source model used in this calculation gives  $K = 0.84$  and  $\kappa = 1.30$  for reproducibility  
352 of tsunami height in the wide area along the coast of Thailand (Suppasri et al., 2011). Therefore, it can  
353 be said that this calculation has the same tsunami reproducibility as the previous study.



354

355 Figure 5 Topographic change and shoreline position caused by the tsunami (solid & dashed lines show  
 356 that the coastline after and before the tsunami in the simulation, P and Q are the points confirmed local  
 357 beach erosion in region (a) and (b), blue and red mapping show erosion and deposition after the  
 358 tsunami in the simulation)

359

### 360 3.1.2. Shoreline changes

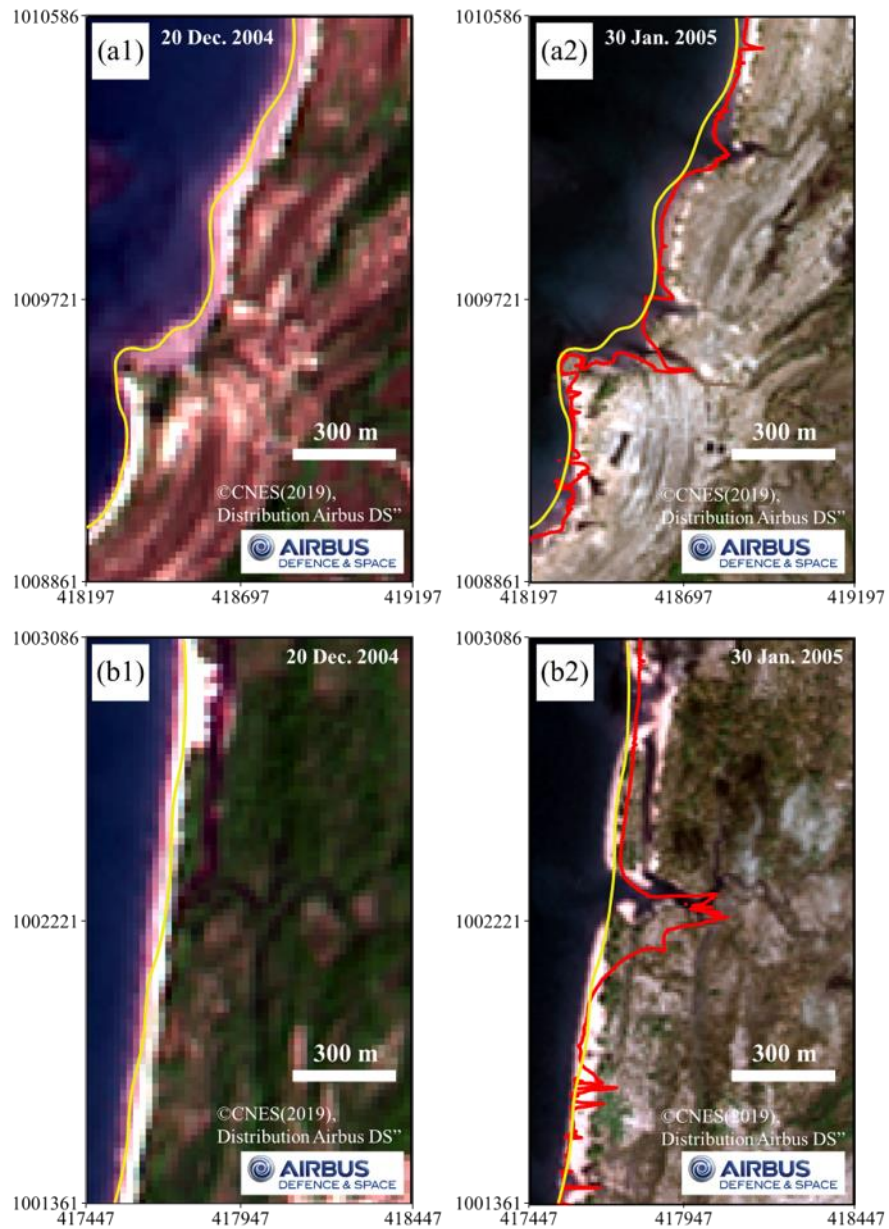
361 Our sediment transport models identify the locations of significant sediment erosion, which are con-  
 362 firmed from post-tsunami satellite images. Figure 5 shows the pre-2004 IOT topographical and geo-  
 363 morphological features (dashed line) and the modelled changes caused by the tsunami (solid line). Ero-  
 364 sion typically occurs locally where small tidal channels breach the youngest beach ridge system (Figure  
 365 5(a) and 5(b)). Comparison with the satellite image shows that the position of erosion in both regions  
 366 is consistent (Figure 6). Although the actual amount of erosion is unknown, this indicates that the planar  
 367 spread of the eroded component can be well reproduced by the calculation. Region (a) was further  
 368 investigated in detail, as the area corresponds to the point where sediment outflow occurred (Jankaew  
 369 et al., 2008).

370

371

372



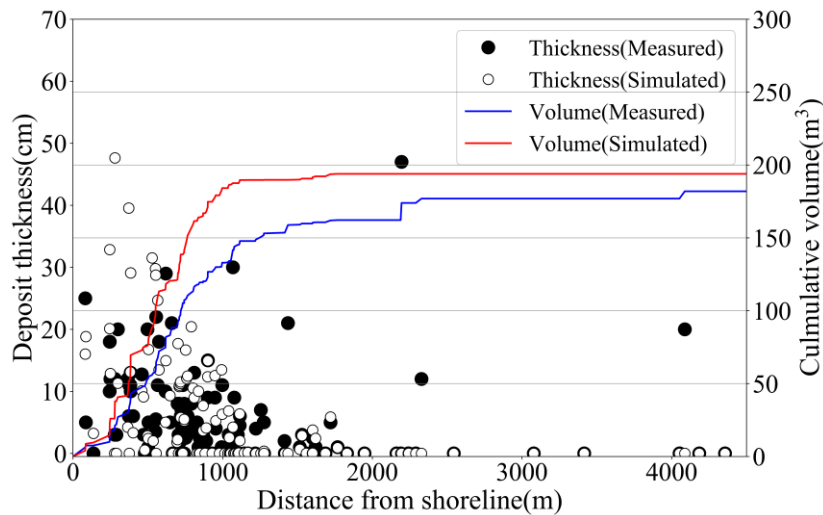


373  
 374  
 375  
 376  
 377  
 378  
 379  
 380  
 381  
 382  
 383  
 384  
 385

Figure 6 Comparison of observed shoreline position from Figure 5 region (a) and (b) derived from satellite images before and after the tsunami (20 Dec. 2004 and 30 Jan. 2005), which is overlain by the modelled extent of erosion showing that the modelled results closely match the observed changes. The red line is the calculated shoreline after the tsunami, and the yellow line is the shoreline before the tsunami (© CNES, 2019, Distribution Airbus DS™).

a1) Satellite image before the tsunami in region (a), a2) Satellite image after the tsunami in region (a),  
 b1) Satellite image before the tsunami in region (b), b2) Satellite image after the tsunami in region (b)





386  
387  
388  
389  
390  
391

Figure 7 Comparison of field measured and simulated tsunami deposit thickness using a representative grain size of  $d = 0.127$  mm. Black point shows the measured thickness by Jankaew et al. (2008) and Gouramanis et al. (2017), white point shows the simulated thickness. Blue and red line show the cumulative curves of measured data and simulated data.

### 3.1.3. 2004 IOT onshore sediment deposition

393  
394  
395  
396  
397  
398  
399

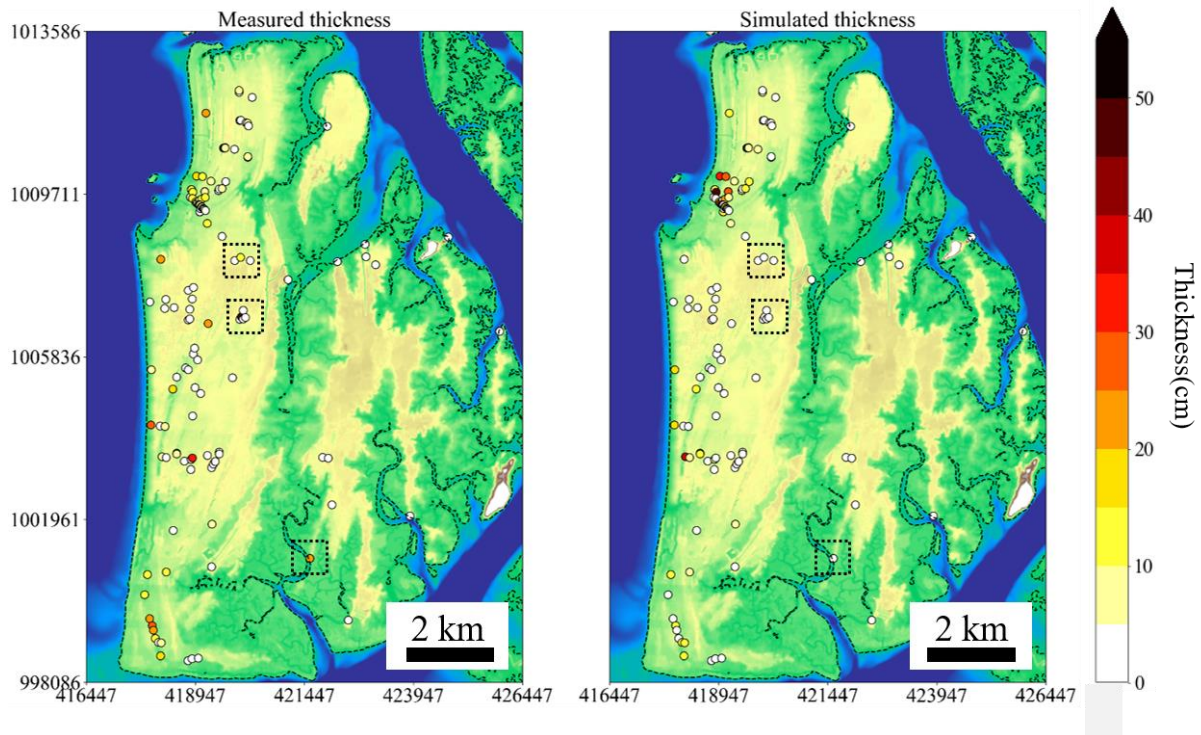
In addition to the erosional features, the model simulated the deposition of 2004 IOT sediments across the island. The thickness of these simulated deposits is compared with 133 measured 2004 IOT deposit thicknesses (Jankaew et al., 2008; Gouramanis et al., 2017). Figure 7 shows a comparison of layer thicknesses at each site (black circles for measured results and white circles for simulated results), which shows that most of the sites are overestimated within 1 km from the shoreline and underestimated at distances greater than 2 km from the shoreline. The model specification and topographical data can be considered as the major causes of this error.

400  
401  
402  
403  
404  
405  
406  
407  
408

First, considering the overestimation within 1 km of the inundation distance, it is found that the STM has a setting of the maximum suspended concentration,  $C_{max}$  as 37.7% (Xu, 1999a and 1999b). The computed suspended concentration in this area is higher than  $C_{max}$ . Therefore, the surplus sediment is forced to be deposited in this zone causing overestimation. Pham et al. (2018) found that the source of tsunami deposits in Phra Thong Island is mainly the sediment from the nearshore zone. In other words, the first wave, which had the highest wave height, eroded a large amount of sediment in the nearshore and transported a large amount of sediment inland. Therefore, it is considered that the maximum concentration was reached during the first wave run-up because of the very high concentration of suspended sediment, which led to the overestimation of the forced sedimentation in the simulation.

409  
410  
411  
412  
413

Second, considering the underestimation of the deposition in inundation distances of 2 km or more, the most likely reason is the computational grid and the model specification. Previous studies have shown that tsunami deposits are highly affected by locality features (e.g. Sugawara et al., 2014a; Watanabe et al., 2018). As shown in three locations with the actual measured deposit thickness (dashed boxes) in Fig. 8, it can be seen that most of the measured thickness is zero which indicate and support



414

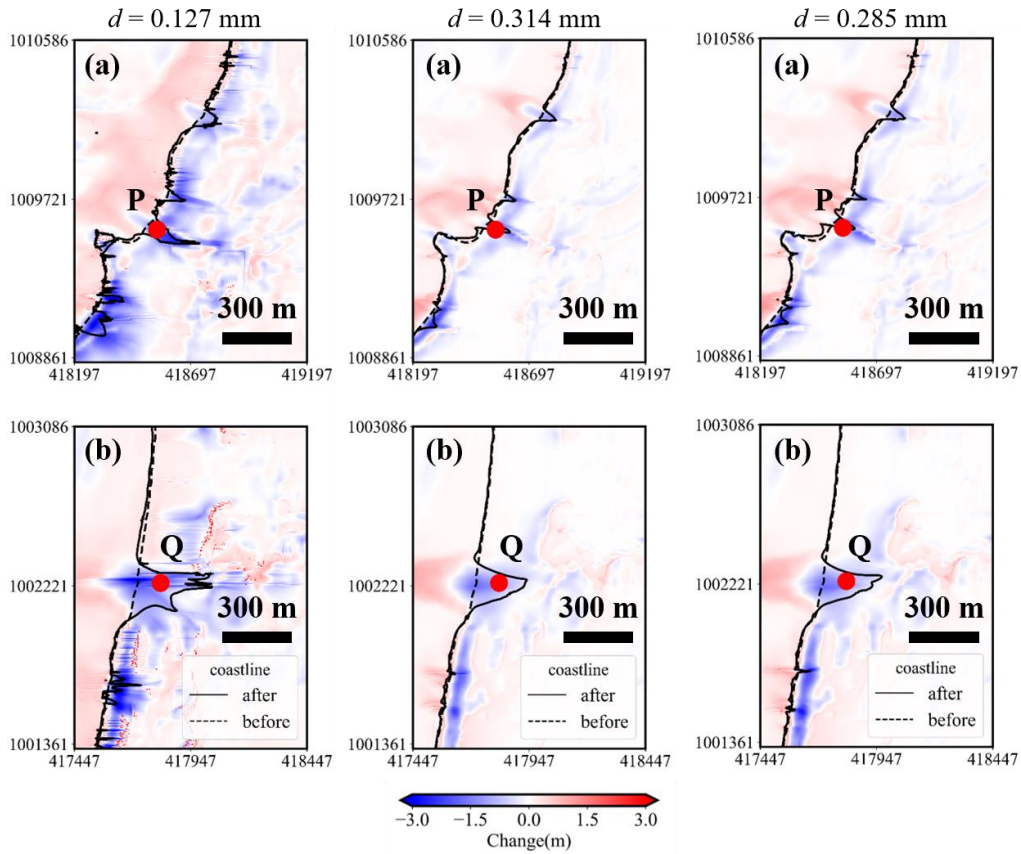
415 Figure 8 Spatial distribution of measured and simulated thickness of tsunami deposits. The black dotted  
 416 lines indicate that the calculated values are underestimated at distances greater than 2 km.

417

418 the reasons of localized deposition. Although the computational grid is very fine ( $\Delta x_6 = 5$  m), it is dif-  
 419 ficult to reproduce local sedimentation with averaged elevation data. **It is worth noting that STM adopts**  
 420 **only single grain size and can only perform deposits which consist sand.** Sugawara et al. (2014a) con-  
 421 ducted tsunami sediment transport simulation on the Sendai Plain and discussed the transportation pos-  
 422 sibility of finer grained sandy and muddy sediment. Muddy sediments were also found in the Sendai  
 423 Plain at a distance of 2 km or more from the 2011 tsunami. Sugawara et al. (2014a)'s STM-based tsu-  
 424 nami sediment transport simulation could not be reproduced for Phra Thong Island. **This can be attribute**  
 425 **to the limitation of sandy sediment and single grain size model.** Therefore, it is possible that muddy or  
 426 very fine-grained sediment was deposited at the three sites but were underestimated in the simulations  
 427 using the current model.

428

429 Based on all above-mentioned reasons, it is more practical to evaluate the simulation results by the  
 430 overall trend of the tsunami deposit rather than comparing the thickness point by point. In Figure 7,  
 431 the line of "Cumulative volume" show the cumulative deposition expressed at each point by the sedi-  
 432 ment thickness multiplied by the area of the computational grid. In general, the tsunami deposits are  
 433 greatly affected by local micro-topography (Sugawara et al., 2014a; Jaffe et al., 2016), and it is difficult  
 434 to fit the modelled layer thickness with the observed layer thickness using DEM averaged in a compu-  
 435 tational grid. Therefore, we introduce the concept of cumulative sedimentation, and evaluated the scale  
 436 of the amount of sediment movement generated. Although the modelled layer thickness typically  
 overestimates the observed layer thickness by +7%, such low variation suggests a relatively successful



437

438

439

Figure 9 Topographic change and shoreline position caused by the tsunami for each grain size

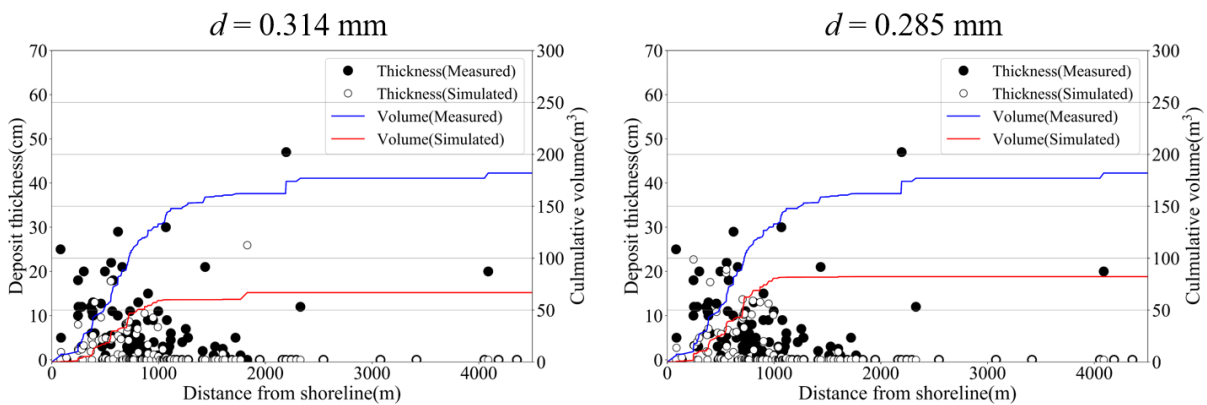
440

Table 3 volume of erosion and deposition in regions (a) and (b) for each grain size (Percentage shows the ratio to reference)

441

	$d$ (mm)	Erosion (m <sup>3</sup> )		Deposition (m <sup>3</sup> )	
		Region (a)	Region (b)	Region (a)	Region (b)
Reference	0.127	352,333	314,189	259,379	254,417
Onshore	0.285	143,793 (41%)	155,225 (49%)	161,810 (62%)	149,470 (59%)
Offshore	0.314	117,491 (33%)	128,289 (41%)	137,749 (53%)	128,801 (51%)

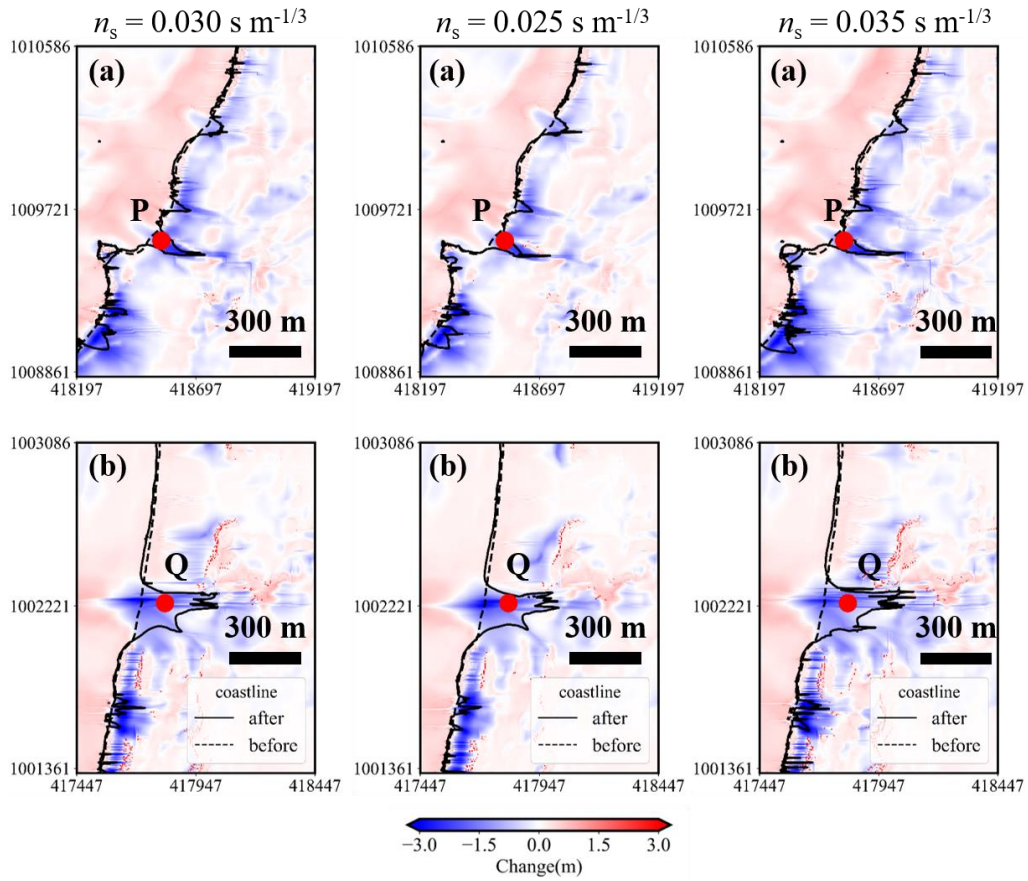
442



443

444

Figure 10 Comparison of field measured and simulated tsunami deposit thickness for each grain size.



445

446

447 Figure 11 Topographic change and shoreline position caused by the tsunami for each roughness coef-  
 448 ficient

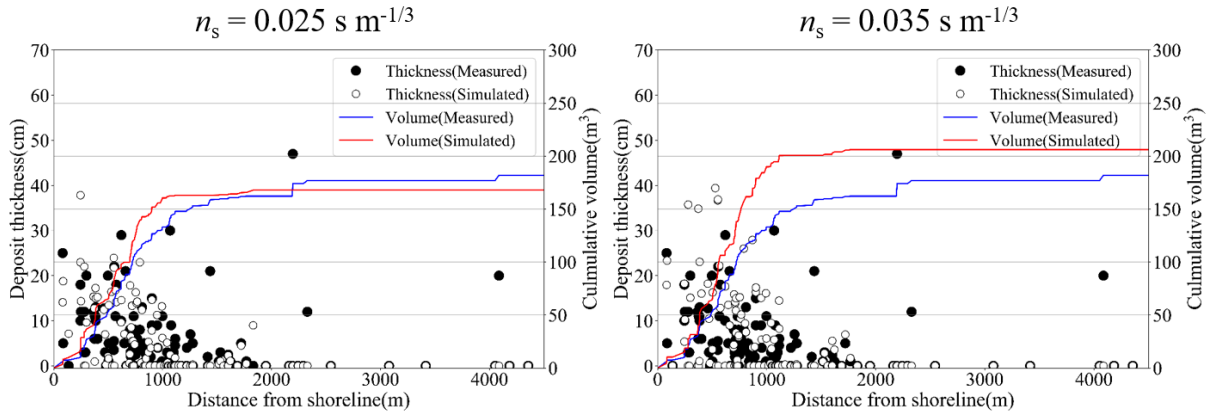
449

450 Table 4 volume of erosion and deposition in regions (a) and (b) for each roughness coefficient (Per-  
 451 centage shows the ratio to reference)

	$n_s$ ( $s m^{-1/3}$ )	Erosion ( $m^3$ )		Deposition ( $m^3$ )	
		Region (a)	Region (b)	Region (a)	Region (b)
Reference	0.030	352,333	314,189	259,379	254,417
Low	0.025	293,032 (83%)	285,659 (91%)	249,242 (96%)	230,905 (91%)
High	0.035	410,323 (116%)	352,284 (112%)	272,394 (105%)	262,522 (103%)

452





453

454 Figure 12 Comparison of field measured and simulated tsunami deposit thickness for each roughness  
 455 coefficient.

456

457 reproduction of the observed dataset (Figure 7). The modelled overestimation is likely due to the as-  
 458 sumption that the entire exposed land area would act as a movable bed. In reality, this is an oversimpli-  
 459 fication of the true ground surface, which contains vegetation that binds and traps the soil and wet  
 460 regions (i.e. in swales) that would have higher degrees of sediment cohesion, reducing the area that  
 461 would be eroded. In addition, the model also reproduces the inland thinning of the 2004 IOT deposit.  
 462 Based on these results, comparison of the sediment layer thickness of the 2004 tsunami shows that the  
 463 scale and the overall sediment transport trend are comparable, and therefore, the results are sufficiently  
 464 reproducible with confidence to evaluate the actual sediment transport.

465

#### 466 3.1.4. Sensitivity analysis for grain size and roughness

467 Figure 9 shows the topographical changes and the thickness of the sediment layers used in this cal-  
 468 culation for each grain size, and Table 3 shows the volume of erosion and deposition in regions (a) and  
 469 (b). These figures show that the smaller the grain size is, the greater the topographic change. This can  
 470 be understood by the smaller the grain size, the larger the Shields parameter in Eq. (10), which indicates  
 471 the ease of sediment transport, and the greater the amount of bed load in Eq. (8). However, Figure 9  
 472 suggests that the qualitative characteristics of sediment transport are the same in the three cases, due to  
 473 the local erosion position of the beach in region (a) and (b) did not change for any grain size. And then,  
 474 comparing the tsunami sediment thickness in Figure 10 the errors of the cumulative volume of  $d = 0.314$   
 475 mm and  $d = 0.285$  mm are -63% and -55%. Therefore, the grain size of  $d = 0.127$  mm is considered to  
 476 show the better reproducibility.

477

478 Figure 11 shows the topographical changes and thickness of sediment layer in this calculation for each  
 479 bottom roughness coefficient, and Table 4 shows the volume of erosion and deposition in regions (a) and (b).  
 480 These figures show that the larger the value of roughness coefficient  $n_s$  is, the greater the topographic  
 481 change. This can be understood by larger the roughness, the larger the Shields parameter in Eq. (10) because  
 482 the friction velocity is proportionate to  $n_s$ . Therefore, an increase in the roughness coefficient indicates the  
 ease of sediment transport, and the greater the amount of bed load in Eq. (8). However, Figure 11 suggests

483 that the qualitative characteristics of sediment transport are the same in the three cases, due to the local  
484 erosion position of the beach in region (a) and (b) did not change for any bottom conditions. And then,  
485 comparing the tsunami sediment thickness in Figure 12, the errors of the cumulative volume of  $n_s = 0.025 \text{ s}$   
486  $\text{m}^{-1/3}$  and  $n_s = 0.035 \text{ s m}^{-1/3}$  are -8% and 13%. Therefore, the roughness coefficient of  $n_s = 0.030 \text{ s m}^{-1/3}$  is  
487 considered to show the better reproducibility.

488

### 489 **3.2. Sediment transport process**

490 Although the model reproduces the zones of sediment erosion and deposition well, the sediment  
491 transport processes during the tsunami event are further examined in regions (a) and (b) in Figure 5.  
492 The modelled time series of the changes of water height and elevation at point P in region (a) and point  
493 Q in region (b) are shown in Figure 13. The modelling results show that the first wave arrived 2 **hours**  
494 **40** minutes after the earthquake, and backwash was generated 10 minutes later (Figure 13). In addition,  
495 the ground surface elevation increased by about 30 cm through sediment deposition during the first  
496 inflowing wave and more than 1.5 m was eroded during the backwash transporting sediment towards  
497 the ocean, so beach loss in both regions is considered to be a result of erosion during the backwash (red  
498 line in Figure 13).

499 In addition, no major topographic changes occurred on the beaches in both areas after the second  
500 wave backwashed, most of the sediment movement on the eroded beaches is considered to have been  
501 completed by the second wave drawback. In other words, the sediment transport processes during this  
502 period are the most important to examine the shoreline changes that occurred during the tsunami and  
503 set up the primary conditions for beach recovery post-tsunami. As such, there are two narrow time  
504 periods that highlight the key factors that for establishing the initial conditions of the recovery process.  
505 First, why was not the beach eroded by the inflowing waves? Second, how did the sediment flowing  
506 seaward in the first wave move?

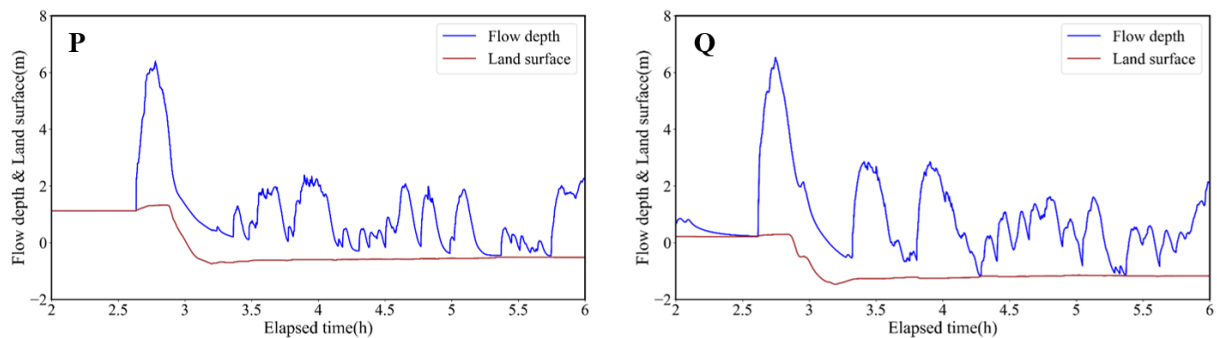
507 Based on the waveform (which assumes a flat surface), a shore-normal cross section calculation was  
508 carried out along the transect in Figure 2. The transect covers the region (b) from **1,000 m** offshore  
509 across the shoreline and **1,000 m** inland. Beyond these distances the planar effect was considered to be  
510 negligible. Figure 14 shows the changes in ground level, water level, suspended sediment concentration  
511 and saturation of suspended sediment concentration on the transect at each unit of time as waves washed  
512 in and out.

513

#### 514 **3.2.1 Why was not the beach eroded by the pushing wave?**

515 As shown in Figure 14, prior to the first wave, the ocean receded to below approximately 8 m below  
516 mean sea level. As inflow of the first wave began, sediment was eroded from the sea floor at **about 5-**  
517 **10m** below mean sea level. This nearshore erosion increased the suspended sediment concentration as  
518 the first wave propagated onshore. At the shoreline, the suspended sediment concentration saturated  
519 and sedimentation could begin at the shoreline. In other words, it is estimated that sediment eroded the  
520 nearshore ( $5 \text{ m} < \text{depth} < 10 \text{ m}$ ) environment during the first inflowing wave, and much of this sediment





521  
 522 Figure 13 Chronological change of flow depth and land surface at point P and Q in region (a) and (b)  
 523 (blue line shows the flow depth and red line shows the land surface)  
 524

525 was transported shoreline and inland.

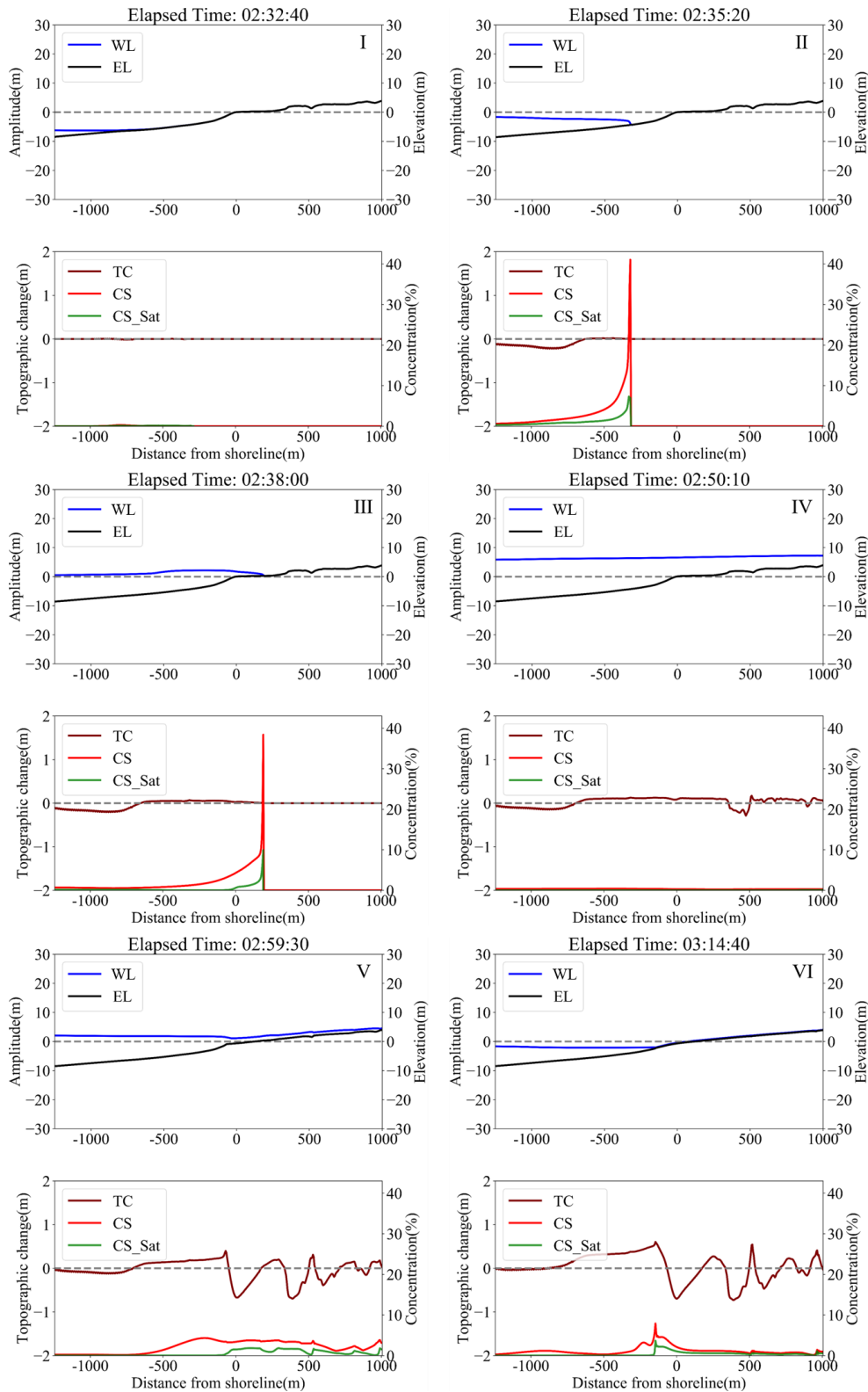
526 It should be noted that, there will be no increase in suspended sediment when the suspended sediment  
 527 is saturated in the model and is the likely reason that the beach was not eroded by the inflowing first  
 528 wave. Although there is a possibility that the beach was actually eroded, the numerical results suggest  
 529 that the erosion in shallow coastal waters (deeper than 5 m but shallower than 10 m) resulted in a very  
 530 high concentration of suspended sediment when the inflowing first wave entered -5 m to the beach  
 531 section of the coast and sediment ceased to be entrained. Pham et al. (2018) found that the source of the  
 532 2004 IOT deposits on Phra Thong Island was from the nearshore (depth < 15 m). This means that large  
 533 scale erosion in shallow water has occurred and a large amount of sediment has been transported inland  
 534 which agrees with the simulation results. Therefore, it is highly likely that the sediment concentration  
 535 was very high when it reached the beach during the **first** inflowing wave. Takahashi (2012) showed that  
 536 when the suspended sediment is in a high concentration state, turbulence is suppressed and the ability  
 537 to retain suspended sediment may decrease. Therefore, it is highly probable that the same phenomenon  
 538 occurred on Phra Thong Island and the beach erosion during the inflowing wave was suppressed.

539

### 540 **3.2.2 How did the sediment flowing seaward in the first wave move?**

541 In Figure 14, at the initiation of backwash, the suspended sediment concentration is low. As backwash  
 542 flows towards the ocean, the velocity increases, which increases erosion and causes the suspended sed-  
 543 iment concentration to increase. This finding is consistent with the changes recorded in Figure 13. Beach  
 544 erosion due to backwash has also been confirmed in for the 2004 IOT in Sri Lanka and the 2011 Tsunami  
 545 along the Sendai Plain and at Rikuzentakata. (e.g. Tanaka et al., 2007, Tanaka et al. 2011, Yamashita et  
 546 al. 2015, 2016). On the Sendai Plain, the estuary section of the old river tends to increase the return  
 547 flow due to the tsunami (Tanaka et al., 2007, Tanaka et al. 2011). Therefore, there is a possibility that  
 548 the region (a) and (b) (Fig. 2, 5 and 6) where local beach erosion of the backwash occurred on Phra  
 549 Thong Island are the old river part.

550 Conversely, the entire beach was eroded by the return flow in Rikuzentakata (Yamashita et al., 2015,  
 551 2016), but no erosion was observed along the entire beach on Phra Thong Island and the Sendai Plain.  
 552 Yamashita et al. (2015, 2016) suggested that the difference between Rikuzentakata and the Sendai Plain



553

554

555

556

557

558

Figure 14 Change in water level (WL), land surface (EL), topographic change (TC), suspended sediment concentration (CS), and saturation suspended sediment concentration (CS\_Sat) by section calculation along the survey line in region (b). ( I ) before the first inflowing wave, ( II ) Advance of first leading wave in shallow water, ( III ) Start of first leading wave run-up, ( IV ) Maximum of first leading wave , ( V ) Advance of second backwash, ( VI ) Maximum of second backwash

559 may be related to the horizontal distance of the plains. On the Sendai Plain, the inland topographic  
560 gradient is small, the inundation distance is long and the inland inundation depth tends to be small.  
561 Therefore, the potential energy that the inundation depth changes to kinetic energy during the backwash  
562 (return flow) becomes relatively small. The Sendai Plain and Phra Thong Island are flooded plains over  
563 2 km inland and have similar topographical features.

564 From the above reasons, the local beach erosion due to the return flow on Phra Thong Island occurred  
565 at the mouths of tidal channels and within tidal channels and that minimal erosion occurred across the  
566 wider beach ridge strand plain. As backwash of the first wave ended, the water still contained a high  
567 suspended sediment concentration and this was deposited in the nearshore environment at less than 5  
568 m water depth (Figure 15). After that, no significant topographic change was found. Thus, this model-  
569 ling shows that most of the sediment that eroded from the onshore area was deposited in the shallow  
570 nearshore zone.

571

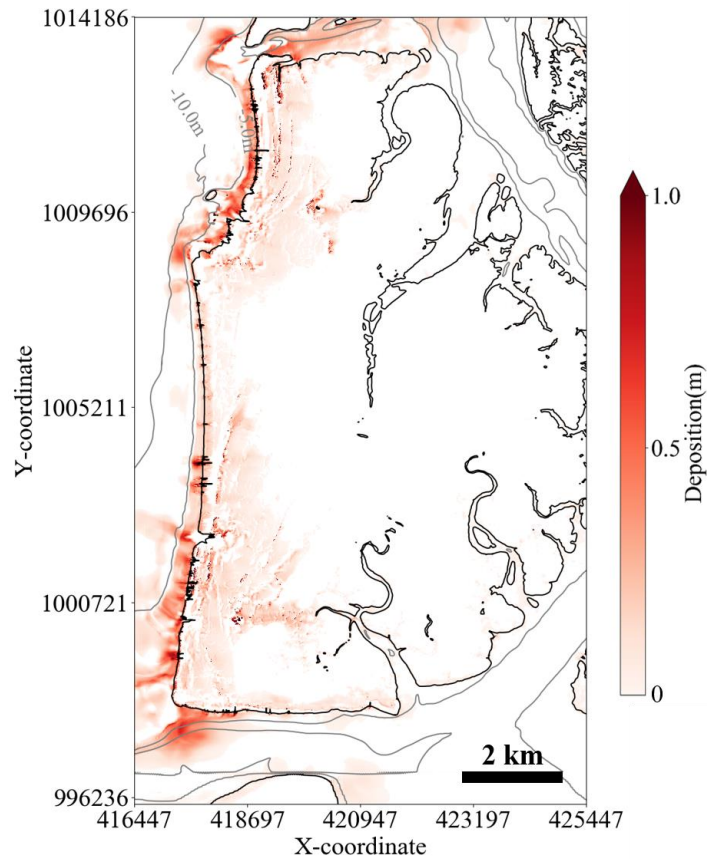
## 572 **4. Discussion**

### 573 **4.1. *Sediment transport process and beach erosion***

574 Regions (a) and (b) were selected for detailed investigation of the simulation results and discussed.  
575 On Phra Thong Island, the 2004 IOT wave was large enough to expose the nearshore sediments and  
576 entrained most of its sediments from the shallow offshore region (below 5m). The wave ran up the  
577 exposed nearshore area while retaining sediment from the shallow offshore region. The sediment con-  
578 centration gradually increases as the wave runs up the relatively long distance of the exposed nearshore  
579 zone, and became sediment-saturated as the wave reached the shoreline, making it difficult for new  
580 sediment to be eroded further. This explains why there was little erosion of the beach during the inflow-  
581 ing wave, and may be a characteristic sediment transport property of shallow beaches like those on Phra  
582 Thong Island. The numerical simulation results suggest that there is little transportation of sediments  
583 from beach by the first inflowing wave and that inland tsunami deposits originated from the nearshore  
584 environment. This finding validates Sawai et al. (2009)'s observation that the 2004 IOT entrained dia-  
585 toms from shallow offshore waters at Phra Thong Island, and Pham et al. (2018)'s observation that  
586 sediment grain sizes and mineralogy were most similar to those of nearshore sediments. Figure 15  
587 shows the results of the calculated sediment deposition both onshore and offshore Phra Thong Island.  
588 From the modelling results, most of the eroded sediment was deposited in shallow nearshore environ-  
589 ments in water less than approximately 5 m deep.

590 The simulations show that the eroded sediments were deposited in the nearshore zone during back-  
591 wash (Fig. 15), which primed the coastal zone for rapid coastal recovery. The removal of sediment from  
592 the onshore coastal zone also generated accommodation space that may have contributed to the coastal  
593 recovery process. Future studies can build on these findings to determine the extent of sediment  
594 transport and deposition, and identify the processes of coastal recovery on Phra Thong Island.

595 Geomorphologically, the Sendai Plain, which was inundated by the March 11, 2011 Great East Japan  
596 tsunami, is similar to the beach ridge plain on Phra Thong Island (Tanaka et al., 2011), but most of the



597  
 598 Figure 15 Sediment distribution derived from the simulation (showing depth contours at 5 m intervals  
 599 in the sea area)

600  
 601 tsunami sediment deposited onshore came from terrestrial sources (Goto et al., 2012; Szczuciński et al.,  
 602 2012; Takashimizu et al., 2012; Sugawara et al., 2014b). However, the Great East Japan tsunami differed  
 603 from the 2004 IOT as the Japanese event had a much smaller receding wave (Nationwide Ocean Wave  
 604 information network for Ports and HARbourS, NOWPHAS; available at  
 605 <http://www.milt.go.jp/kowan/nowphas>). As such the Japanese tsunami may not have achieved sediment  
 606 saturation as the wave approached the shoreline, thereby containing a lower sediment concentration and  
 607 allowing large volumes of sediment to be entrained from the beach for subsequent formation of inland  
 608 deposits. The different sources of deposited sediment in the two areas reflect contrasting sediment  
 609 transport mechanisms on shallow beaches, and may be useful for identifying paleotsunami from coastal  
 610 recovery and geological records.

611  
 612 **4.2. Limits of calculation results**

613 This study analyzed tsunami sediment transport on Phra Thong Island using numerical calculations  
 614 and assumed that the island was unvegetated and lacked topography. However, the western half of the  
 615 island has an undulating surface caused by the beach ridge and swale system, and is extensively vege-  
 616 tated with trees and dense grasses on the ridges and thick grasses within the swales. The eastern half of  
 617 the island has wide tidal channels and an extensive fringing mangrove system. Both topography and

618 differing vegetation types add complexity to the inundation and backflow sediment transport models  
619 not captured here. In future, it is necessary to consider the influence of **vegetation and topography** on  
620 tsunami sediment transport.

621 Another potential limitation of the model is the selection of a single (median) grain size for the sed-  
622 iments. As shown in previous studies (e.g. Sugawara et al., 2014a, b), the assumption of transport of  
623 single grain sized sediment differs from actual situations because of the distribution of grain sizes **mo-**  
624 **bilized** and deposited by tsunami. Therefore, it is important to set representative grain sizes and fully  
625 study how grain size affects tsunami sediment transport. Future modelling may consider simulating the  
626 suite of grain sizes individually or simulating a population of grain sizes that are identified in the modern  
627 environment and in preserved tsunami deposits.

628 Furthermore, although the calculation was performed considering the entire area a movable bed, the  
629 existence of fixed beds, such as rocky areas, should be considered. We consider this a minor component  
630 of this research as the rocky headlands that serve as fixed beds are relatively small in area and would  
631 contribute little to the overall simulations in our models.

632 Sugawara et al. (2014b) considers the simulation result of sediment layer thickness using the tsunami  
633 sediment transport calculation to be affected by grain size, bottom conditions and topographic data.  
634 Their study showed that the layer thickness increases as grain size becomes finer and the layer thickness  
635 distribution tendency was unchanged regardless of grain size. Similar results were obtained in this study.

636  
637

## 638 **5. Conclusion**

639 Because of insufficient knowledge about the topographic recovery process after a tsunami, this study  
640 used sediment transport modelling to identify the erosional and depositional processes affecting the  
641 coastal zone at Phra Thong Island, Thailand during the 2004 Indian Ocean Tsunami.

642 First, it was confirmed by comparing simulated results of the shoreline and sediment layer thickness  
643 that the location of beach runoff identified on Phra Thong Island was reproducible and consistent with  
644 sediment transport results (Figs. 6 and 7). Based on the sediment transport results we conclude that the  
645 processes of sediment erosion and deposition on Phra Thong Island are characterized by the following  
646 sequence:

- 647 • erosion caused by the inflowing waves occurred at a relatively shallow location in the offshore  
648 area and the transported sediment was deposited near the shoreline;
- 649 • the inflowing waves caused minimal erosion of the shoreline; and,
- 650 • erosion of the shoreline was largely caused by backwash resulting in onshore sediments depos-  
651 ited in the shallow nearshore zone.

652 These erosional and depositional processes demonstrate the locations of sediment removal and sub-  
653 sequent deposition during the different phases of the first tsunami wave on Phra Thong Island which  
654 will serve as an important baseline of sediment sources for further study of the recovery process. The  
655 simulations also show that the zones of erosion and deposition across the island and offshore coastal

656 zone are non-uniform. In particular, the zones of erosion and deposition highlighted in the simulations  
657 establish the environmental conditions that existed in the transitional phase between catastrophic tsu-  
658 nami and normal coastal processes that facilitated coastal recovery.

659

660

## 661 **6. Acknowledgements**

662 We would like to express our gratitude for the support from Dr. Panon Latcharote of the **Faculty of**  
663 **Engineering, Mahidol University**, Prof. Supot Teachavorasinskun, Dean of Faculty of Engineering,  
664 Chulalongkorn University, Dr. Pitcha Jongvivatsakul, Department of Civil Engineering Chulalongkorn  
665 University; and data from the Royal Thai Navy. RM, AS, KY, FI was support by JSPS Grant-in-Aid for  
666 Scientific Research (A) No. 17H01631 (FY2017 - FY2021). AS and NL was support by JSPS Bilateral  
667 program for joint research with National Research Council of Thailand (NRCT) (FY2017 - FY2018).  
668 CG was supported by NUS grant (R-109-000-223-133). NL was supported by Ratchadapisek Sompoch  
669 Endowment Fund (2019), Chulalongkorn University (762003-CC). This work is a contribution to IGCP  
670 Project 639, ‘Sea-level Change from Minutes to Millennia’.

671

## 672 **References**

- 673 1) Abe, T., Goto, K., and Sugawara, D.: Relationship between the maximum extent of tsunami sand  
674 and the inundation limit of the 2011 Tohoku–oki tsunami on the Sendai Plain, Japan, *Sedimentary*  
675 *Geology*, 282, 142–150, 2012.
- 676 2) Aida, I.: Reliability of a tsunami source model derived from fault parameters, *J. Phys. Earth*, 26,  
677 57–73, 1978.
- 678 3) Ali, P. Y., and Narayana, A. C.: Short-term morphological and shoreline changes at Trinkat Island,  
679 Andaman and Nicobar, India, after the 2004 tsunami. *Marine Geodesy*, 38(1), 26-39, 2015.
- 680 4) Arimitsu, T., Kawasaki, K., and Nimura, M.: Numerical simulation of sediment transport and bot-  
681 tom topography change due to tsunami with large scale eddy, *Journal of JSCE, B2 (Coastal Engi-  
682 neering)*, 73, 2, 643–648, 2012.
- 683 5) Apotsos, A., Buckley, M., Gelfenbaum, G., Jaffe, B., and Vatvani, D.: Nearshore tsunami inunda-  
684 tion model validation: toward sediment transport applications. *Pure and Applied Geophysics*, 168,  
685 2097-2119, 2011a.
- 686 6) Apotsos, A., Gelfenbaum, G., and Jaffe, B.: Process-based modeling of tsunami inundation  
687 and sediment transport, *Journal of Geophysical Research*, 116, F01006, 2011b.
- 688 7) Apotsos, A., Gelfenbaum, G., Jaffe, B., Watt, S., Peck, B., Buckley, M., and Stevens, A.: Tsunami  
689 inundation and sediment transport in a sediment-limited embayment on American Samoa: *Earth-  
690 Science Reviews*, 107, 1-11, 2011c.
- 691 8) Bagnold, R. A.: An approach to the sediment transport problem from general physics. US govern-  
692 ment printing office, 1966.
- 693 9) Brill, D., Klasen, N., Jankaew, K., Brückner, H., Kelletat, D., Scheffers, A., and Scheffers, S.: Local



- 694 inundation distances and regional tsunami recurrence in the Indian Ocean inferred from limines-  
695 sence dating of sandy deposits in Thailand, *Natural Hazards and Earth System Sciences*, 12, 2177–  
696 2192, 2012a.
- 697 10) Brill, D., Klasen, Brückner, H., Jankaew, K., Scheffers, A., Kelletat, D., and Scheffers, S.: OSL  
698 dating of tsunami deposits from Phra Thong Island, Thailand, *Quaternary Geochronology*, 10, 224–  
699 229, 2012b.
- 700 11) Brill, D., Jankaew, K., Bruckner, H.: Holocene evolution of Phra Thong's beach-ridge plain (Thai-  
701 land) — Chronology, processes and driving factors, *Geomorphology*, 245, 117–134, 2015.
- 702 12) ChaguéGoff, C., Andrew, A., Szczuciński, W., Goff, J., and Nishimura, Y.: Geochemical signa-  
703 tures up to the maximum inundation of the 2011 Tohoku–oki tsunami — Implications for the 869  
704 AD Jogan and other palaeotsunamis, *Sedimentary Geology*, 282, 65–77, 2012.
- 705 13) Choowong, M., Phantuwongraj, S., Charoentitirat, T., Chutakositkanon, V., Yumuang S., and Cha-  
706 rusiri, P.: Beach recovery after 2004 Indian Ocean tsunami from Phang–nga, Thailand, *Geomor-  
707 phology*, 104, 134–142, 2009.
- 708 14) Fagherazzi, S. and Du, X.: Tsunamigenic incisions produced by the December 2004 earthquake  
709 along the coasts of Thailand, Indonesia and Sri Lanka, *Geomorphology*, 99, 120–129, 2008.
- 710 15) Feldens, P., Schwarzer, K., Szczuciński, W., Stattegger, K., Sakuna, D. and Sompongchaiykul, P.  
711 Impact of 2004 tsunami on seafloor morphology and offshore sediments, Pakarang Cape, Thailand,  
712 *Polish Journal of Environmental Science* Vol. 18, No. 1, 63-68, 2009.
- 713 16) Fujino S., Naruse H., Matsumoto, D., Jarupongsakul T., Sphawajruksakul A., and Sakakura, N.:  
714 Stratigraphic evidence for pre–2004 tsunamis in southwestern Thailand, *Marine Geology*, 262, 25–  
715 28, 2009.
- 716 17) Fujino, S., Naruse, H., Matsumoto, D., Sakakura, N., Suphawajruksakul, A., and Jarupongsakul,  
717 T.: Detailed measurements of thickness and grain size of a widespread onshore tsunami deposit in  
718 Phang–nga Province, southwestern Thailand, *Island Arc*, 19, 389–398, 2010.
- 719 18) Gelfenbaum G., Vatvani D., Jaffe B., and Dekker F.: Tsunami inundation and sediment transport  
720 in vicinity of coastal mangrove forest, *Coastal Sediments*, 07, 1117-1128, 2007.
- 721 19) Goto, K., Takahashi, J., Oie, T., and Imamura, F.: Remarkable bathymetric change in the nearshore  
722 zone by the 2004 Indian Ocean tsunami: Kirinda Harbor, Sri Lanka, *Geomorphology*, 127, No.1-  
723 2, 107–116, 2011a.
- 724 20) Goto, K., ChaguéGoff, C., Fujino, S., Goff, J., Jaffe B., Nishimura, Y., Richmond, B., Sugawara,  
725 D., Szczuciński, W., Tappin, R. D., Witter, C. R., and Yuliant, E., New insights of tsunami hazard  
726 from the 2011 Tohoku–oki event, *Marine Geology*, 290, 46–50, 2011b.
- 727 21) Goto, K., ChaguéGoff, C., Goff, J., and Jaffe, B.: The future of tsunami research following the  
728 2011 Tohoku–oki event, *Sedimen- tary Geology*, 282, 1–13, 2012.
- 729 22) Gouramanis, C., Switzer, A. D., Polivka, P. M., Bristow, C. S., Jankaew, K., Dat, P. T., Pile, J.,  
730 Rubin, C. M., Yingsin, L., Ildefonso, S. R., and Jol, H. M.: Ground penetrating radar examination  
731 of thin tsunami beds - A case study from Phra Thong Island, Thailand, *Sediment. Geol.*, 329, 149–

- 732 165, 2015.
- 733 23) Gouramanis, C., Switzer, A. D., Jankaew, K., Bristow, C. S., Pham, D. T., and Ildefonso, S. R.:  
734 High-frequency coastal overwash deposits from PHRA thong Island, Thailand, *Sci. Rep.*, Vol.7,  
735 No. September 2016, 1–9, 2017.
- 736 24) Gusman, A. R., Tanioka, Y., and Takahashi, T.: Numerical experiment and a case study of sediment  
737 transport simulation of the 2004 Indian Ocean tsunami in Lhok Nga, Banda Aceh, Indonesia., *Earth,*  
738 *planets and space*, 64, 817-827, 2012.
- 739 25) Haraguchi, T., Takahashi, T., Hisamatsu, R., Morishita, Y., and Sasaki, I.: A Field Survey of Geo-  
740 morphic Change on Kessenuma Bay caused by the 2010 Chilean Tsunami and the 2011 Tohoku  
741 Tsunami, *Journal of JSCE, B2 (Coastal Engineering)*, 68, 231–235, 2012.
- 742 26) Hawkes, A.D., Bird, M., Cowie, S., Grundy-Warr, C., Horton, B.P., Hwai, A.T.S., Law, L., Mac-  
743 gregor, C., Nott, J., Ong, J.E., Rigg, J., Robinson, R., Tan-Mullins, M., Sa, T.T., Yasin, Z., Aik,  
744 L.W.: Sediments deposited by the 2004 Indian Ocean Tsunami along the Malaysia–Thailand Pen-  
745 insula, *Marine Geology*, 242, 169–190, 2007.
- 746 27) Hirao, R., Tanaka, H., Umeda, M., Adityawan, M. B., Mano, A., and Udo, K.: Breaching of Sandy  
747 Coast and Spit Due To The 2011 Tsunami and Their Recovery, *Journal of JSCE, B2(Coastal Engi-*  
748 *neering)*, 68, 581–585, 2012.
- 749 28) Imai, K., Sugawara, D., Takahashi, T., Iwama, S., and Tanaka, H.: Numerical study for sediment  
750 transport due to tsunami around the Kitakami River mouth, *Journal of JSCE, B2(Coastal Engineer-*  
751 *ing)*, 71, 247–252, 2015.
- 752 29) Imamura, F.: Review of tsunami simulation with a finite difference method, in: *Long-Wave Runup*  
753 *Models*, edited by: Yeh, H., Liu, P., and Synolakis, C. E., World Scientific Publishing Co., Singa-  
754 pore, 25–42, 1996.
- 755 30) Iwagaki, Y.: Hydrodynamical study on critical tractive force, *Trans. JSCE*, 41(41), 1–21, 1956.
- 756 31) Jaffe, B., Goto, K., Sugawara, D., Gelfenbaum, G., and La Selle, S.: Uncertainty in tsunami sedi-  
757 ment transport modeling. *Journal of Disaster Research*, 11(4), 647-661, 2016.
- 758 32) Jankaew, K., Atwater, B. F., Sawai, Y., Choowong, M., Charoentitirat, T., Martin, M. E., and Pren-  
759 dergast, A.: Medieval forewarning of the 2004 Indian Ocean tsunami in Thailand, *Nature*,  
760 455(7217), 1228–1231, 2008.
- 761 33) Koiwa, N., Takahashi, M., Sugisawa, S., Ito, A., Aki Matsumoto, H., Tanavud, C., and Goto, K.:  
762 Barrier spit recovery following the 2004 Indian Ocean tsunami at Pakarang Cape, southwest Thai-  
763 land, *Geomorphology*, 306, 314–324, 2018.
- 764 34) Land Development Department of Thailand (LDD) Maps and mapping information, Available at:  
765 [http://www.ddd.go.th/www/lek\\_web/web.jsp?id=19273](http://www.ddd.go.th/www/lek_web/web.jsp?id=19273) (Accessed date: 18 October 2017)
- 766 35) Li, L., Qiu, Q., and Huang, Z.: Numerical modeling of the morphological change in Lhok Nga,  
767 west Banda Aceh, during the 2004 Indian Ocean tsunami: understanding tsunami deposits using a  
768 forward modeling method, *Natural Hazards*, 64, 1549-1574, 2012.
- 769 36) Li, L., Huang, Z., and Qiu, Q.: Numerical simulation of erosion and deposition at the Thailand

- 770 Khao Lak coast during the 2004 Indian Ocean tsunami, *Natural Hazards*, 74, 2251-2277, 2014.
- 771 37) Liew, S.C., Gupta, A., Wong, P.P., Kwoh, L.K.: Recovery from a large tsunami mapped over time:  
772 The Aceh coast, Sumatra, *Geomorphology*, 114, 520–529, 2010.
- 773 38) Morishita, Y., and Takahashi, T.: Accuracy improvement of movable bed model for tsunamis by  
774 applying for Kesennuma bay when the 2011 Tohoku tsunami arrived, *Journal of JSCE, B2(Coastal*  
775 *Engineering)*, 70, 491–495, 2014.
- 776 39) Rubey, W. W.: Settling velocity of gravel, sand, and silt particles. *American Journal of Science*,  
777 148, 325-338, 1933.
- 778 40) Saegusa, S., Tanaka, H., and Mitobe, Y.: Recovery processes of bathymetry of Sendai Bay after the  
779 2011 tsunami, *Journal of JSCE, B2(Coastal Engineering)*, 73, 817–822, 2017.
- 780 41) Okada, Y.: Surface deformation due to shear and tensile faults in a half-space, *Bulletin of the Seis-*  
781 *mological Society of America*, 75(4), 1135–1154, 1985.
- 782 42) Pari, Y., Ramana Murthy, M. V., Jaya Kumar, S., Subramanian, B. R., and Ramachandran, S.: Mor-  
783 phological changes at Vellar estuary, India — Impact of the December 2004 tsunami, *Journal of*  
784 *Environmental Management*, 89, 45–57, 2008.
- 785 43) Paris, R., Lavigne, F., Wassmer, P., Sartohadi, J.: Coastal sedimentation associated with the De-  
786 cember 26, 2004 tsunami in Lhok Nga, west Banda Aceh (Sumatra, Indonesia), *Marine Geology*,  
787 238, 93–106, 2007.
- 788 44) Pham, T. D., Gouramanis, C., Switzer, M. A., Rubin, M. C., Jones, G. B., Jankaew, K., and Carr,  
789 F. P.: Elemental and mineralogical analysis of marine and coastal sediments from Phra Thong Is-  
790 land, Thailand: Insights into the provenance of coastal hazard deposits, *Marine Geology*, 385, 274–  
791 292, 2018.
- 792 45) Prendergast, L. A., Cupper L. M., Jankaew, K., and Sawai, Y.: Indian Ocean tsunami recurrence  
793 from optical dating of tsunami sand sheets in Thailand, *Marine Geology*, 295–298, No.15, 20–27,  
794 2012.
- 795 46) Sawai, Y., Jankaew K., Martin, E. M., Prendergast, A., Choowong, M., and Charoentitirat, T.: Di-  
796 atom assembles in tsunami deposits associated with the 2004 Indian Ocean tsunami at Phra Thong  
797 Island, Thailand, *Marine Micropaleontology*, 73, 70–79, 2009.
- 798 47) Sugawara, D., Goto, K., and Jaffe, B. E.: Numerical models of tsunami sediment transport –Current  
799 understanding and future directions, *Marine Geology*, 352, 295–320, 2014a.
- 800 48) Sugawara, D., Takahashi, T., and Imamura, F.: Sediment transport due to the 2011 Tohoku-oki  
801 tsunami at Sendai: Results from numerical modeling, *Mar. Geol.*, 358, 18–37, 2014b.
- 802 49) Suppasri, A., Koshimura, S., and Imamura, F.: Developing tsunami fragility curves based on the  
803 satellite remote sensing and the numerical modeling of the 2004 Indian Ocean tsunami in Thailand,  
804 *Nat. Hazards Earth Syst. Sci.*, 11(1), 173–189, 2011.
- 805 50) Suppasri, A., Latcharote, P., Bricker, J. D., Leelawat, N., Hayashi, A., Yamashita, K., Makinoshima,  
806 F., Roeber, V. and Imamura, F.: Improvement of tsunami countermeasures based on lessons from  
807 the 2011 great east japan earthquake and tsunami -Situation after five years-, *Coastal Engineering*

- 808 Journal, 58 (4), 1640011, 2016.
- 809 51) Switzer, A.D., Srinivasalu, S., Thangadurai, N., Ram Mohan, V.: Bedding structures in Indian tsunami deposits that provide clues to the dynamics of tsunami inundation, Geological Society, London, Special Publications, 361, 61-77, 2012.
- 810  
811
- 812 52) Szczuciński, W., Kokociński, M., Rzeszewski, M., Chahué–Goff, C., Cachão, M., Goto, K., and Sugawara, D.: Sediment sources and sedimentation processes of 2011 Tohoku–oki tsunami deposits on the Sendai Plain, Japan — Insights from diatoms, nannoliths and grain size distribution, *Sedimentary Geology*, 282, 40–56, 2012.
- 813  
814  
815
- 816 53) Takahashi, T., Shuto, N., Imamura, F., and Asai, D.: Modeling sediment transport due to tsunamis with exchange rate between bed load layer and suspended load layer, *Proceedings Of International Conference of Coastal Engineering*, 1508–1519, 2000.
- 817  
818
- 819 54) Takahashi, J., Goto, K., Oie, T., Yanagisawa, H., and Imamura, F.: Inundation and topographic Change due to the 2004 Indian Ocean Tsunami at the Kirinda port, Sri Lanka, *Journal of JSCE, B2(Coastal Engineering)*, 55, 251–255, 2008.
- 820  
821
- 822 55) Takahashi, T., Kurokawa, T., Fujita, M., and Shimada, H.: Hydraulic experiment on sediment transport due to tsunamis with various sand grain size, *Journal of JSCE, B2(Coastal Engineering)*, 67, 231–235, 2011.
- 823  
824
- 825 56) Takahashi, T.: Numerical modeling of sediment transport due to tsunamis and its problem, *Journal of the Sedimentological Society of Japan*, 71, 2, 149-155, 2012.
- 826
- 827 57) Takashimizu, Y., Urabe, A., Suzuki, K., and Sato, Y.: Deposition by the 2011 Tohoku–oki tsunami on coastal lowland controlled by beach ridges near Sendai, Japan, *Sedimentary Geology*, 282, 124–141, 2012.
- 828  
829
- 830 58) Tanaka, H., Ishino, K., Nawarathna, B., Nakagawa, H., and Yano, S.: Coastal and river mouth morphology change in Sri Lanka due to the 2004 Indian Ocean Tsunami. In *Coastal Sediments' 07* (pp. 842-855), 2007.
- 831  
832
- 833 59) Tanaka, H., Mano, A., and Udo, K.: Beach Morphology Change Induced by The 2011 Great East Japan Earthquake Tsunami, *Journal of JSCE, B2(Coastal Engineering)*, 67(2), 571–575, 2011.
- 834
- 835 60) Udo, K., Tanaka, H., Mano, A., and Takeda, Y.: Beach Morphology Change of Southern Sendai Coast due to 2011 Tohoku Earthquake Tsunami, *Journal of JSCE, B2(Coastal Engineering)*, 69, 391–395, 2013.
- 836  
837
- 838 61) Udo, K., and Takeda, Y.: Comparison between characteristics of shoreline changes due to the 2004 Indian Ocean tsunami and the 2011 Great East Japan tsunami, *Journal of JSCE, B3(Coastal Engineering)*, 72, 175–180, 2016.
- 839  
840
- 841 62) Van Rijn, L. C.: Unified view of sediment transport by currents and waves. I: Initiation of motion, bed roughness, and bed-load transport. *Journal of Hydraulic engineering*, 133(6), 649-667, 2007.
- 842
- 843 63) Watanabe, A., Maruyama, Y., Shimizu, T., and Sakakiyama, T.: Numerical prediction model of three-dimensional beach transformation due to installed structures, *Journal of JSCE(Coastal Engineering)*, 31, 406–410, 1984.
- 844  
845

- 846 64) Watanabe, M., Goto, K., Bricker, J. D., and Imamura, F.: Are inundation limit and maximum extent  
847 of sand useful for differentiating tsunamis and storms? An example from sediment transport simu-  
848 lations on the Sendai Plain, Japan. *Sedimentary geology*, 364, 204-216, 2018.
- 849 65) Xu, J.: Grain-size characteristics of suspended sediment in the Yellow River, China, *Catena*, 38,  
850 243-263, 1999a.
- 851 66) Xu, J.: Erosion caused by hyperconcentrated flow on the Loess Plateau of China, *Catena*, 36, 1-19,  
852 1999b.
- 853 67) Yamashita, K., Sugawara, D., Takahashi, T., Imamura, F., Saito, Y., Imato, Y., Kai, T., Uehara, H.,  
854 Kato, T., Nakata, K., Saka, R., and Nishikawa, A.: Numerical simulation of large-scale sediment  
855 transport due to the 2011 tohoku earthquake tsunami in Rikuzentakata city, *Journal of JSCE*,  
856 B2(Coastal Engineering), 71, 499–504, 2015.
- 857 68) Yamashita, K., Sugawara, D., Takahashi, T., Imamura, F., Saito, Y., Imato, Y., and Saka, R.: Nu-  
858 merical simulations of large-scale sediment transport caused by the 2011 Tohoku Earthquake Tsu-  
859 nami in Hirota Bay, Southern Sanriku Coast. *Coastal Engineering Journal*, 58(04), 2016.
- 860 69) Yamashita, K., Shigihara, Y., Sugawara, D., Arikawa, T., Takahashi, T., and Imamura, F.: Effect of  
861 sediment **transport** on tsunami hazard and building damage –an integrated simulation of tsunami  
862 inundation, sediment transport and drifting vessels in Kesenuma city, Miyagi prefecture during  
863 the great east Japan –, *Journal of JSCE*, B2(Coastal Engineering), 73, 355–360, 2017.
- 864 70) Yamashita, K., Sugawara, D., Arikawa, Y., Takahashi, T., and Imamura, F.: Improvement of tsu-  
865 nami-induced sediment transport model by considering saturated concentration in suspension with  
866 strong unsteady flows, *Journal of JSCE*, B2(Coastal Engineering), 69, 325–330, 2018.
- 867 71) Yunus Ali, P., and Narayama, A. C.: Short–Term Morphological and Shoreline Changes at Trinkat  
868 Island, Andaman and Nicobar, India, After the 2004 Tsunami, *Marine Geodesy*, 38, 26–39, 2015.
- 869